Deep Water Transport By Acoustic-Gravity Waves Generated By Submarine Earthquakes

Author: Mohammed Alghazi

Supervisor: Dr. Usama Kadri

Submitted: November 2023

Revised: November 2023

Submitted for the degree of Ph.D. in Mathematics

School of Mathematics
Cardiff University,
Senghennydd Road,
Cardiff,
CF24 4AG,
Wales, U.K.

Acknowledgements

I commence by expressing my profound gratitude to Allah, the Most Merciful and Most Compassionate. It is through the grace and blessings of Allah that I have found the strength, guidance, and inspiration to navigate the challenges of this academic journey. I offer my deepest thanks for the wisdom, resilience, and the opportunity to pursue knowledge and personal growth.

I extend my heartfelt gratitude to my supervisor, Usama Kadri, for his constant encouragement, guidance, and support throughout this academic journey. His mentorship has been invaluable. I'm particularly thankful for his exceptional support during the challenging times since the birth of my baby who has been fighting for her life. Kadri's understanding and unwavering encouragement provided me with the strength and motivation to continue my research, even in the face of personal adversity. His dedication to my academic development, coupled with his constructive feedback, enriched my work and significantly contributed to my accomplishments. I am deeply appreciative of his extraordinary support and privileged to have him as my supervisor.

I extend my heartfelt gratitude to my parents for their unwavering support and belief in me. Their constant encouragement and love have been my greatest source of motivation throughout this academic journey.

I extend my heartfelt gratitude to my beloved wife, Lama, for her unwavering support and love. Her presence has been a constant source of motivation and strength throughout this academic journey. I want to express my deep appreciation to my 6-year-old daughter, Hesseh, for her boundless love and her bright and understanding spirit. Her innocent encouragement and the love she shares have been a source of inspiration to me on this academic journey.

I'm especially thankful for my 2-year-old baby, Najd, who has shown incredible strength throughout her numerous surgeries and her remarkable journey to survival. Her unwavering resilience and determination have taught me the invaluable lesson of perseverance. She has been a profound source of inspiration, and I am profoundly grateful for her presence in my life.

I would like to extend my heartfelt gratitude to my family for their continuous sup-

port and belief in my endeavours. Their encouragement and unwavering support have played an essential role in my academic journey. I am deeply thankful for the love and unity that my family has provided me, making this achievement possible.

A special thanks goes to Byron Williams, who has not only been a good colleague but also an outstanding friend. His assistance with derivations and coding has been instrumental in the success of this work. Byron's expertise and dedication have made a significant difference in the completion of this project.

I want to express my sincere thanks to Yazeed, Hassan, Bernabe, Ahlam, Layla, Saeideh, and Rabin for their collaboration, fellowship, and friendship throughout this academic journey. Their support has been invaluable.

I offer a heartfelt thank you to Dr. Ibrahim Althobaiti, a Neurosurgery and Epilepsy Consultant, whose expertise, dedication, and help were crucial in saving my baby's life more than once. His exceptional contributions provided not just medical care but also hope during such challenging times. We are profoundly grateful for his support and lifesaving efforts.

I extend my sincere gratitude to the Saudi Government, the Ministry of Education, Majmaah University, the Royal Embassy of Saudi Arabia in London, and the Saudi Cultural Bureau in London for their generous support of my studies. Their financial and educational support has been essential in enabling me to pursue my academic goals.

Summary

The assumption that the ocean is incompressible has been carried out in the vast majority of research on deep ocean currents which is reasonable in some applications. An incompressible ocean with an average depth h has for every frequency ω and wave number κ only one progressive wave which is the gravity wave. However, taking compressibility into account gives m progressive wave modes for every frequency ω for horizontal wave numbers k_n where $n = 0, 1, ..., m$ and k_0 is almost equal to the gravity wave in the incompressible case. These waves, known as Acoustic-Gravity Waves (AGWs), are progressive types of waves generated among others by the interaction between wind and wave, submarine earthquake, and other sources with amplitudes governed by the restoring force of gravity [21] [54]. Similarly to other well-known water drifting mechanisms, AGWs may play an important role in creating deep currents in the ocean and transporting water, which are vital for the healthness of the oceans. Although this mechanism has been demonstrated qualitatively, it is still not known how much water is being transported compared to other mechanisms. To this end, we study the role of AGWs generated by submarine earthquakes and estimate the amount of water transferred by these waves. It is found that AGWs play a prominent role in transporting water to various locations in the ocean [22].

CONTENTS

LIST OF FIGURES

LIST OF TABLES

Chapter 1

Introduction

1.1 General background

Currents are movements of water bodies that are driven by various forces, leading to the transfer of different properties to the water [53] which plays an important role in human being life [22]. Different types of regular and irregular movements of water in the oceans that transfer temperature and salinity are represented by ocean currents [32] [43]. Rahmstorf [37] indicates that there are two main mechanisms for the generation currents. One is the wind, as it blows over the ocean's surface it increases the water inertia which causes a current. The other mechanism concerns high and low temperatures or evaporation and precipitation which lead to convection currents. Ferrari and Wunsch [16] [53] agree that winds and tides in the water almost govern the oceanic general circulation and huge energy is given to the ocean by the wind despite that some of the energy disappears within 100 m of the surface. Other mechanisms are also considered such as tidal force, rotation of the earth, energy from the sun, and movement of animals in the ocean [48] [11]. The highest source of energy transferred to the ocean surface is gained from the wind [16] where the action of winds converts the kinetic energy directly to oceanic kinetic and potential energy where the net transfer of the energy was estimated in the range of 7-36 TW where most of the energy is kept on the surface and starts a turbulent mixing and produce surface gravity waves [53]. The water reaches deep regions of the ocean carrying the properties of the surface water with high density

down. According to [53] the water sinks about 1000 m in the ocean with a net mass flux rate of 25-30 $\times 10^9$ kg/s. This turbulent mixing with thermohaline force is the main reason for Thermohaline circulation [53]. Although the two circulations are forced by two different mechanisms, the circulations are not separated as any change of the wind stress would change the thermohaline circulation and vice versa. These circulations affect climate change and understanding its behaviour is very important to understand climate change [37].

1.1.1 Surface currents

Surface currents occur in the upper ocean layers (400 m below the ocean surface, which is 10% of the average ocean depth), influenced primarily by wind patterns, and they can extend for long distances, shaping vast oceanic basins. Surface currents are vital oceanic movements near the water's surface, driven by wind, temperature, salinity, and Earth's rotation. They create complex flows that impact marine ecosystems, weather patterns, and global heat distribution. These currents are driven by different forces such as winds that are generated by atmospheric pressure differences thus initiating surface currents. The Coriolis effect, due to Earth's rotation, deflects the moving water masses, causing curved paths known as gyres. Coastlines, underwater topography, and temperature and salinity gradients also influence their direction and intensity. Surface currents play a vital role in redistributing heat globally, affecting coastal climates, and they also interact with atmospheric systems, influencing weather patterns. Surface currents also transport nutrients, plankton, and larvae, impacting marine ecosystems and supporting fisheries. [16].

1.1.2 Deep currents

Deep currents occur in the lower layers of the ocean (more than 400 m below the ocean surface) and they are essential for the Earth's oceanic circulation. Unlike surface currents, they are driven by temperature and salinity variations and earthquakes [37]. These currents play a significant role in redistributing heat, nutrients, and carbon dioxide throughout the global oceans as they flow beneath the ocean's surface, extending thou-

sands of meters below resulting in the transport of large volumes of water. temperature and salinity differences in the ocean surface form a current known as Thermohaline circulation where cold, dense water sinking near the polar regions initiates the downward flow relying on the cooling of surface waters and the formation of deep water masses. Changes in salinity, such as from freshwater input, can alter the density and flow of deep currents [37]. Deep currents regulate global climate patterns by redistributing heat from the equatorial regions to higher latitudes. They also transport nutrients and support marine ecosystems through upwelling, bringing nutrient-rich waters to the surface. These currents have a critical function in storing carbon dioxide, preserving a portion of it, and contributing to the regulation of the global climate.

1.2 Carbon cycle

The carbon cycle in the ocean plays a critical role in the Earth's system, with approximately 50% of carbon being transferred from the atmosphere to the ocean [20]. Phytoplankton, a primary component of the oceanic ecosystem, utilize this carbon as a nutrient source, and their consumption by marine animals further contributes to the carbon flow [42]. Upon the death of phytoplankton, their organic matter sinks to the deep ocean, where carbon is dissolved and made available for utilization by small marine organisms that are unable to swim against ocean currents [22][39]. These interconnected cycles, including the carbon cycle, are crucial for the overall health of the ocean and the Earth, relying on ocean currents to facilitate the transport of carbon and other essential elements between different oceanic layers [42].

1.3 Sediments

In deep-sea environments, sediment accumulation doesn't solely depend on the rain of particles from above. Instead, the movement of bottom currents can redistribute these particles, leading to selective accumulation in certain areas, a phenomenon known as "sediment focusing." Changes in this focus can cause fluctuations in sediment accumulation rates, independent of variations in particle supply from above. This highlights

the potential impact of deep water transport on sediment transportation in deep-sea environments, emphasizing the importance of understanding these processes for interpreting sediment records and assessing environmental changes over time [46].

1.4 Stokes drift

The motion of a fluid can be described using either Lagrangian, which follows a fluid particle as it travels, or Eulerian, which is observed by looking at the flow at every point at different times [33]. Hence, Stokes drift velocity is obtained by the difference between the mean Lagrangian velocity of a fluid particle and the mean Eulerian of a flow at a specific point [22]. Stokes drift, driven by ocean waves, has a significant impact on oceanic drift. Understanding its characteristics and mechanisms is crucial for comprehending the movement of water particles, the dispersion of substances, and the functioning of coastal ecosystems.

1.5 Tectonic plates movements

The earth is a construction shaped by four layers: inner core, outer core, mantle, and crust. The inner core of the earth is solid and has a thickness of about 1278 km while the outer core is liquid and it's about 2200 km in thickness. The mantle lays on the core and it is about 2800 km in thickness while the crust is the thinnest layer by 0-100 km in thickness [12]. The crust of the earth is composed of two types: (1) Oceanic which is the crust where the oceans lay and (2) Continental which forms the land. The solid outer shell of the earth is called the Lithosphere and it is divided into tectonic plates that move constantly at a rate of about 0.6 inches a year [40]. Tectonic plates are fundamental components of the Earth's lithosphere, comprising large, rigid pieces that fit together like a jigsaw puzzle and cover the Earth's surface. These plates are in constant motion, driven by forces within the Earth's interior [34]. There are three primary types of tectonic plate boundaries: divergent boundaries, convergent boundaries, and transform boundaries, each characterized by distinct geological processes and features [30].

1.5.1 Divergent boundary

Divergent boundaries occur where tectonic plates move apart from each other forming gaps or rifts that allow magma from the underlying asthenosphere to rise, filling the void and solidifying as new crust. These boundaries are most observed along mid-ocean ridges, where oceanic plates are spreading apart. As the new crust forms, it pushes the existing plates on either side away, resulting in the expansion of the ocean basin. Divergent boundaries are also responsible for the formation of rift valleys on land, such as the East African Rift System [3].

1.5.2 Convergent boundary

Convergent boundaries arise from plate collisions. This movement bends the edge of the plates, or at least one of them, up into a formation of the mountain range. In some cases, it bends one of the plates down into a deep seafloor trench. Convergent boundaries can be characterized as oceanic-oceanic, oceanic-continental, or continental-continental. The oceanic-oceanic convergence subducts the denser plate, forming trenches and volcanic activity. Oceanic-continental convergence leads to volcanic arcs and uplifted crust, resulting in mountain ranges. Continental-continental convergence causes intense deformation, folding, and uplift, creating extensive mountain belts[3].

1.5.3 Transform boundary

Transform boundaries are characterized by plates sliding past one another horizontally. These boundaries are sites of intense shearing and the release of seismic energy, often resulting in frequent earthquakes. The most famous transform boundary is the San Andreas Fault in California, where the Pacific Plate and the North American Plate slide past each other. Transform boundaries accommodate the lateral motion between two plates, allowing them to move independently. Unlike divergent and convergent boundaries, transform boundaries do not create or destroy crust[3].

1.6 Global impact

Tectonic plate movement is involved in shaping the Earth's geological features and has significant implications for the distribution of land and the formation of oceanic basins. Plate boundaries, where tectonic plates interact, exhibit dynamic activities such as earthquakes, the uplift of mountain ranges, the formation of oceanic trenches, and volcanic processes [35]. These processes play a crucial role in the recycling of rocks from the Earth's mantle, facilitating the transport of vital nutrients and minerals essential for sustaining life. Volcanic activity associated with plate boundaries not only contributes to the availability of surface water but also has implications for atmospheric processes [29]. It is important to note that plate movement is a primary factor in the occurrence of tsunamis. Underwater earthquakes release enormous amounts of energy, which propagates through the water as a tsunami, a powerful and far-reaching oceanic wave phenomenon.

1.7 Fault proprieties

Faults are fractures in the Earth's crust resulting from rock movement. Their properties offer insights into geological dynamics. Key fault characteristics include:
1) Orientation: The fault plane's angle and direction compared to surrounding rock layers. This reveals past tectonic movements and stress patterns.
2) Displacement: Measures rock movement along the fault plane. It indicates earthquake potential and contributes to understanding tectonic history.
3) Activity: Fault movement status. Active faults pose seismic risks due to recent movement, while inactive faults are less hazardous.
4) Length and Width: Longer faults accumulate more strain and energy, impacting earthquake potential and deformation distribution.
Studying these properties informs seismic hazard evaluation and enhances the understanding of the earth's crustal processes.

1.8 Research objectives

The research objective of this study is to determine and quantify the volumetric rate of deep-water drifting caused by AGWs generated by submarine earthquakes. This investigation aims to establish a comprehensive understanding of the dynamics and impact of these waves on ocean currents and water displacement. By employing advanced modelling techniques such as Stokes drift and stationary phase approximation and analyzing relevant seismic events, this research provides insights into the complex interactions between seismic activity, AGWs propagation, and their important effects on oceanic processes, contributing to an enhanced comprehension of submarine earthquake-induced phenomena and their broader implications for oceanography and geophysics.

1.9 Research outlines

Chapter 1: Introduces the research by highlighting the significance of ocean dynamics, outlining the research objectives, and emphasizing the broader environmental impact.
Chapter 2: Provides the foundational knowledge required for understanding the subsequent research. It covers essential concepts, including the mass continuity equation, Euler equation, wave equation, stationary phase approximation, and surface waves. The chapter delves into the properties of seismic waves and surface gravity waves, which are vital for the study's theoretical framework.
Chapter 3: Introduces AGWs and delves into their effects on deep ocean currents, employing a 2D orbital velocity analysis.
Chapter 4: in this chapter the modelling of deep water transport driven by AGWs generated by submarine earthquakes is carried out. This includes an analysis of the inverse envelope equation, and derivatives of the envelope factor, and employs the stationary-phase approximation for large time scales.
Chapter 5: In this chapter, equations are derived to quantify water transport by AGWs generated by submarine earthquakes. Gravity's impact on wave dynamics and particle motion is presented, followed by a detailed exploration of Lagrangian particle motions, Stokes drift velocities in water waves, the dynamics of Lagrangian particle motion, and a discussion of Taylor's expansion for drift velocity. Horizontal drift velocity and mean

Stokes drift velocity are then delved into to arrive at the model to quantify water transport by AGWs generated by submarine earthquakes.

Chapter 6: Research findings are presented in this chapter, focusing on a case study of the Sumatra earthquake's submarine fault. An analysis of water transport dynamics, including a whole-depth analysis and an in-depth examination of different depth layers, is provided. The results shed light on the intricate interplay of water transport by AGWs and the contributions of each mode in various depths.

Chapter 7: Diving into the key findings and their implications, the focus is on water transport by AGWs and the results showed that this type of wave contributes in transporting water in all depths. The influence of AGWs and their impact is discussed. The main contributions of the research are highlighted, emphasising the role of this study in advancing the understanding of the ocean dynamics and water transport driven by AGWs generated by geological forces.

Chapter 2

Foundation

2.1 Background

Water transport in the deep ocean is a complex and vital process that plays a significant role in Earth's climate system, influencing global temperature regulation, oceanic circulation patterns, and the distribution of heat and nutrients throughout the planet's interconnected ecosystems. It involves various mechanisms, including density gradients, currents, and water masses. Thermohaline circulation, driven by variations in temperature and salinity, influences the vertical and horizontal movement of water masses [37]. Wind-driven currents, such as the Antarctic Circumpolar Current, contribute to the overall water transport in the deep ocean [45]. Mesoscale eddies, formed by the interaction of different water masses, enhance mixing and redistribute water properties [9].

Water masses, characterized by distinct temperature, salinity, and nutrient content, are key components of deep ocean circulation [44]. Examples include North Atlantic Deep Water (NADW) and Antarctic Bottom Water (AABW). NADW forms through deep convection in the North Atlantic, while AABW is generated through the sinking of dense water masses in the Antarctic region [16] [41].

The implications of deep-water transport are significant on a global scale. It plays a crucial role in redistributing heat and regulating Earth's climate. Deep-water upwelling brings nutrient-rich waters to the surface, stimulating primary productivity and support-

ing diverse marine ecosystems [8]. Deep-water transport also contributes to the storage and sequestration of carbon dioxide, aiding in mitigating climate change [10]. Furthermore, deep-water circulation patterns are interconnected with other oceanic processes, including the formation of oceanic fronts and the modulation of sea surface temperatures [36].

To enhance our understanding of water transport in the deep ocean, ongoing research utilizing advanced observational techniques and modelling approaches is necessary. High-resolution oceanographic measurements, remote sensing technologies, and numerical simulations provide insights into the intricate dynamics of deep-water circulation [38]. Integration of these approaches helps refine our knowledge of the physical processes and their implications for climate variability and change.

2.2 Mass continuity equation

The mass continuity equation is a mathematical expression that describes how a conserved mass is transported. Landau, L. D. and Lifshitz, E. M. [26] state that the mass continuity equation, also known as the mass conservation equation, arises from calculating the net mass flow through a fluid cube over a specific time period:

$$\frac{\partial \rho}{\partial t} + div(\rho \vec{v}) = 0 \tag{2.2.1}$$

where ρ denotes the fluid's density, $\vec{v}$ is the fluid's velocity, and $div(\rho\vec{v})$ is the rate of change of the mass density of the fluid as it flows. In situations where there is minimal motion amplitude, like in sound waves, the variations in pressure and density are relatively small [17]. Consequently, it is possible to express the density ρ and pressure P as follows:

$$\begin{aligned} P &= P_0 + P', \\ \rho &= \rho_0 + \rho'. \end{aligned} \tag{2.2.2}$$

Here, P_0 and ρ_0 represent the constant equilibrium values, while P' and ρ' denote the small deviations from the equilibrium state. By substituting equations (2.2.2) into the continuity equation (2.2.1) and disregarding the second-order terms of ρ' and P', the resulting expression is:

$$\frac{\partial \rho'}{\partial t} + \rho_0 \operatorname{div}(\vec{v}) = 0. \tag{2.2.3}$$

Under the assumption of an ideal fluid and adiabatic sound oscillations, a slight change in pressure relates to a slight change in density. Mathematically, this relationship can be represented as

$$P' = \rho' \cdot \left(\frac{\partial P}{\partial \rho_0}\right)_s, \tag{2.2.4}$$

where the s denotes the adiabatic condition. By differentiating equation (2.2.4) and substituting it into equation (2.2.3), the continuity equation can be written into the following form:

$$\frac{\partial P'}{\partial \rho_0} + \rho_0 \cdot \left(\frac{\partial P}{\partial \rho_0}\right)_s \cdot div(\vec{v}) = 0. \tag{2.2.5}$$

2.3 Euler equation

The Euler equation is a fundamental equation in fluid dynamics that describes the motion of an inviscid (non-viscous) fluid. It is derived from Newton's second law of motion applied to a fluid element, allowing us to analyze the dynamics of fluid flow without considering internal friction or viscosity effects [21]. By applying Taylor expansion, the following set of equations is obtained:

$$\frac{\partial \vec{v}}{\partial t} + \left(\vec{v} \cdot \operatorname{grad}\right)\vec{v} = -\frac{1}{\rho}\operatorname{grad}(P), \tag{2.3.6}$$

In the case of small amplitude motion, the magnitude of v is small, allowing us to neglect second-order terms. Consequently, the term $(\vec{v} \cdot \mathbf{grad})\vec{v}$ vanishes from the Euler equation (2.3.6). By substituting equations (2.2.2) into (2.3.6) and disregarding second-

order terms of P' and ρ', the simplified form of the Euler equation is obtained:

$$\frac{\partial \vec{v}}{\partial t} = -\frac{1}{\rho_0}\text{grad}(P'). \tag{2.3.7}$$

2.4 Wave equation

The wave equation is a fundamental equation in fluid dynamics that describes the behaviour of a compressible fluid when it is disturbed from its equilibrium state by showing how the pressure and velocity of the fluid change over time and space. It is used to study a wide variety of phenomena, including sound waves, shock waves, and water waves. It can be derived from the continuity equation and the Euler equation, under the assumption of non-rotational flow [14].

The irritational assumption implies that the velocity can be expressed in the form:

$$\vec{v} = \text{grad}(\phi) \tag{2.4.8}$$

where ϕ is the velocity potential.

Substituting in Euler equation (2.3.7) to get

$$P' = -\rho_0 \cdot \frac{\partial \phi}{\partial t} \tag{2.4.9}$$

Hence, the wave equation can be obtained by inserting (2.4.9) into the continuity equation (2.2.5)

$$\nabla^2 \phi = \frac{1}{c^2}\frac{\partial^2 \phi}{\partial t^2} \tag{2.4.10}$$

where ∇ represents the Laplacian of the scalar field ϕ and c is the speed of sound in the fluid:

$$c = \sqrt{\frac{\partial P}{\partial \rho_0}_s}. \tag{2.4.11}$$

2.5 Stationary phase approximation

The stationary phase approximation is a powerful technique used in various areas of science and mathematics to approximate oscillatory integrals. It is particularly useful when dealing with integrals that exhibit rapid oscillations, making direct evaluation challenging. The principle of the stationary phase approximation lies in identifying the critical points where the phase of the oscillatory integrand remains approximately constant, and then using it to simplify the integral [52]. Consider an oscillatory integral of the form:

$$I(t) = \int_a^b e^{i\phi(t)} f(t)\, dt, \tag{2.5.12}$$

where $\phi(t)$ is a rapidly varying phase function and $f(t)$ is a slowly varying amplitude function. The stationary phase approximation aims to approximate this integral when the phase $\phi(t)$ varies rapidly [5]. The basic idea is to expand the phase $\phi(t)$ around its stationary points, where the derivative $\frac{d\phi}{dt}$ is close to zero. Let's denote one such stationary point as t_0. We then perform a Taylor expansion of the phase function:

$$\phi(t) \approx \phi(t_0) + \frac{1}{2}\phi''(t_0)(t - t_0)^2 + \ldots, \tag{2.5.13}$$

where $\phi''(t_0)$ is the second derivative of the phase at t_0. Substituting this expansion back into the integral, we get:

$$I(t) \approx e^{i\phi(t_0)} \int_a^b e^{i\frac{1}{2}\phi''(t_0)(t-t_0)^2} f(t)\, dt. \tag{2.5.14}$$

The observation is that the exponential term in the integrand is oscillatory only when $\phi''(t_0)$ is non-zero, and it introduces rapid oscillations. However, in the vicinity of t_0, the exponential term varies much slower compared to the oscillations of $f(t)$. Therefore, the integral can be approximated by neglecting the rapid oscillations induced by the exponential term. The stationary phase approximation leads to a significant reduction in the complexity of the integral, and the resulting expression becomes much more manageable to evaluate.

This technique finds applications in a wide range of disciplines, including physics,

engineering, and signal processing, where oscillatory integrals arise in various contexts.

2.6 Surface waves

2.6.1 Seismic waves

Seismic waves are present within the Earth's interior as they traverse through the Earth's layers towards the mantle, giving rise to various natural phenomena such as volcanoes, earthquakes, landslides, and more. Seismic waves are categorized into two main types: body waves, which travel through the Earth's interior, and surface waves, which propagate along the Earth's surface [7]. Surface waves are further divided into two types: Rayleigh waves, named after the mathematician John William Strutt, Lord Rayleigh, who predicted their existence. These waves cause particles to move elliptically in ripples and are also known as ground rolls. The other type is Love waves, named after the mathematician Augustus Edward Hough Love. They result from movements within the Earth's interior, causing particles to move horizontally.

2.6.2 Surface gravity waves

Surface gravity waves are the gravity waves that act on the surface of the water and it's one of the most seen aspects of fluid motions. Surface gravity waves are named so because gravity acts as the restoring force for these waves. It's important to consider the role of Stokes drift, which is the net transport of water in the direction of wave propagation caused by the circular orbits of individual water particles near the surface. Stokes drift is a crucial aspect of these waves.
When the surface of water is forced to rise above the equilibrium surface level and because water is denser than the air, the restoring force, which is gravity, brings it back down. Inertia is gained when the water is falling down, which makes it go under the equilibrium level, and then the bouncing motion results. This phenomenon is often referred to as Stokes drift, where the circular orbits of individual water particles near the surface lead to a net transport of water in the direction of wave propagation.
The mechanisms of fluid waves are nearly the same. The fluid itself is not moving but

it transfers the energy from one area to another, so the fluid is just a medium where the energy is traveling through. That can be clearly seen as a floating object on the water's surface mostly going up and down but not traveling with the wave. This energy, travelling by the surface wave, is eventually dispersed at a certain point and then it has an impact on the water content.
Dhanak, M. and Xiros, N. [15] show that in water of constant depth h, the relation between the frequency and the wavelength is given by the dispersion relation

$$\omega^2 = gk \ \tanh(kh) \tag{2.6.15}$$

where g is the gravitational acceleration and k is the wavenumber and it is expressed as

$$k = \frac{2\pi}{\lambda}. \tag{2.6.16}$$

The wave speed c_p can be written as follows [27]

$$c_p = \frac{\omega}{k} = \sqrt{\frac{g}{k} \ \tanh(kh)}. \tag{2.6.17}$$

In deep water waves, the wavelength is much shorter than the depth. As the wavenumber is very large it means that $kh \gg 1$ hence, $\tanh(kh) \cong 1$. In this case, the dispersion approximation becomes

$$\omega = \sqrt{gk} \tag{2.6.18}$$

thus, the wave speed for deep water waves becomes

$$c_p = \sqrt{\frac{g}{k}} = \sqrt{\frac{g\lambda}{2\pi}}. \tag{2.6.19}$$

In shallow water waves, the wavelength is much longer than the depth Eq.(2.6.15) then becomes

$$\omega = \sqrt{gk^2h} \tag{2.6.20}$$

Then the wave speed can be described as follows

$$c_p = \sqrt{gh}. \tag{2.6.21}$$

For example, a tsunami wave travelling in a 4000 m depth will have a phase speed of 200 m/s or 720 km/hr.

Chapter 3

Acoustic-gravity waves

3.1 Introduction

Acoustic-gravity waves (AGWs) are a type of waves that are generated in a slightly compressible ocean and propagate with amplitudes governed by the restoring force of gravity [50]. These waves can be generated, among others, from the interaction between wind and water surface, submarine earthquake, and other sources [21] [54]. Similar to other mechanisms, AGWs have a contribution in transporting water in the ocean as they can transport water up to a few centimetres per second and this contribution has been demonstrated qualitatively [22]. However, it is still not known how much water is being transported by AGWs compared to other mechanisms. For an incompressible ocean with constant depth h, for any frequency ω there is only a single progressive wave with wave number κ which is the gravity wave [24]. However, in a compressible ocean, there are more than a single progressive wave with wave numbers κ_n for any given frequency ω, where n=0,1,.., N and κ_0 is almost similar to the gravity wave in the incompressible case [24].

To understand the behaviour of the wave we start by introducing the wave equation for the compressible fluid ignoring the gravitational forces in the field interior [31]:

$$\nabla^2\phi = \frac{1}{c^2}\frac{\partial^2\phi}{\partial t^2} \tag{3.1.1}$$

This equation encapsulates the dynamics of waves in a compressible fluid medium where c is the sound speed in water. To further elucidate the context, we integrate the behaviour of waves at both the free surface and the bottom boundary. The combined free surface boundary condition:

$$\phi_{tt} + g\phi_z = 0 \text{ at } z = h \tag{3.1.2}$$

At the free surface, the equation takes into account the acceleration due to gravity and its interaction with the vertical displacement. The free surface boundary condition influences the wave's behaviour as it interacts with the air-water interface.

The bottom boundary condition:

$$\phi_z = w_0(x, z, t) \quad \text{at} \quad z = 0 \tag{3.1.3}$$

At the ocean's bottom, the condition accounts for the disturbance velocity as a function of time and distance. The bottom boundary condition adds another layer of complexity to the wave's behaviour as it encounters the seafloor.

For any acoustic background with a significant water depth h and satisfying the dispersion relation :

$$\omega^2 = g\mu_n \tanh(\mu_n h) \tag{3.1.4}$$

where μ_n are the eigenvalues of the dispersion relation

$$\mu_n^2 = \kappa_n^2 - \frac{\omega^2}{c^2} \tag{3.1.5}$$

This relationship describes the interplay between ω,g, μ_n, and the medium's acoustic properties. Notably, this phenomenon may arise due to the propagation of travelling AGWs, as discussed by Kadri, U. [22].

To explore the implications of the dispersion relation, a graphical solution is pursued. When analyzing the scenario with imaginary values of μ, the dispersion relation

yields a solitary solution as an intersection of $\tanh(\mu h)$ and $\omega^2/g\mu$ as we see in Figure 3.1. Conversely, for real values of μ, the graphical interpretation in Figure 3.2 discloses an infinite array of solutions as intersections of $\tan(\mu h)$ and $-\omega^2/g\mu$.

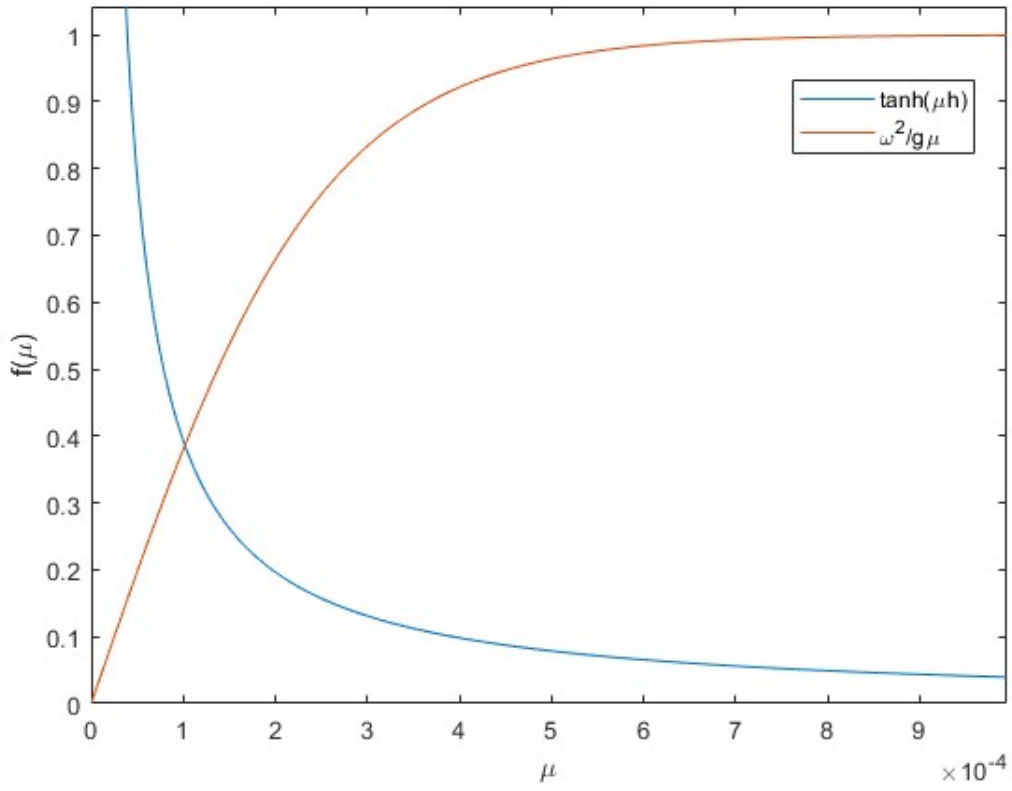

Figure 3.1: Solution of the dispersion relation for imaginary μ for $h = 4000$ m.

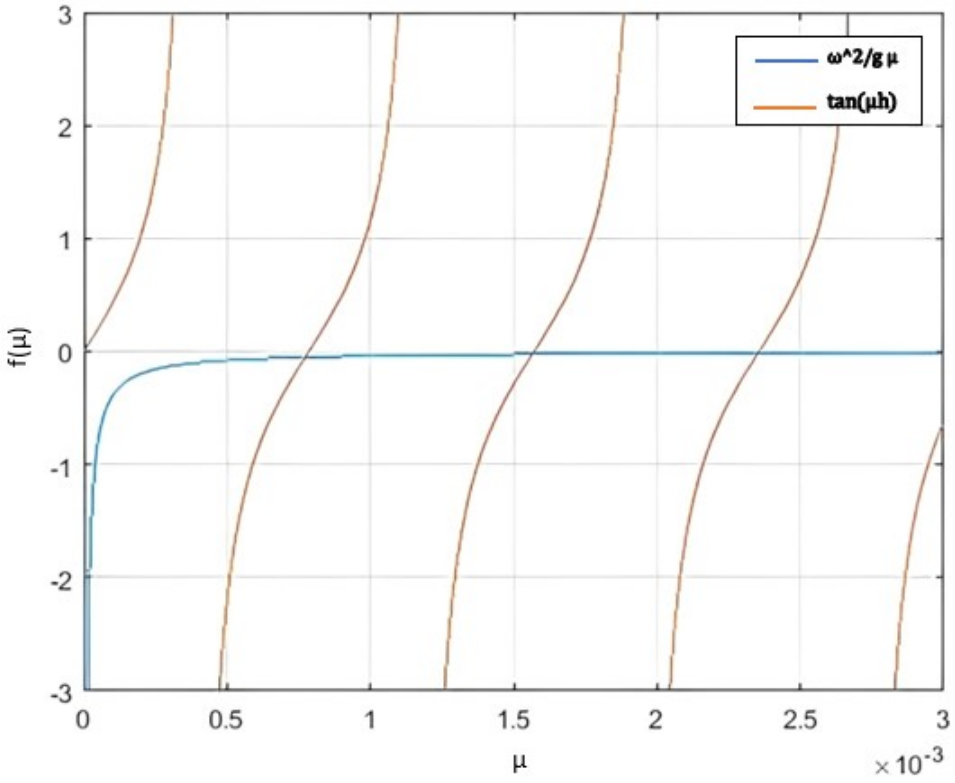

Figure 3.2: Solutions of the dispersion relation for real μ for $h = 4000$ m.

3.2 Deep ocean currents - 2D analysis

To obtain the velocity potential, consider a coordinate system with axes x and z, where the origin is set at the undisturbed free surface and the z-axis directed upward, in this context let $z = -h$ represents the rigid bottom, while $z = \eta$ represents the free surface, taking into account the gravitational forces in the fluid interior from [13]:

$$\frac{\partial^2 \phi}{\partial t^2} - c^2 \nabla^2 \phi + g \frac{\partial \phi}{\partial z} = 0, \qquad -h \leq z \leq \eta \tag{3.2.6}$$

The bottom boundary condition is:

$$\frac{\partial \phi}{\partial z} = 0, \qquad z = -h, \tag{3.2.7}$$

The kinematic boundary condition at the free surface is as follows [28] :

$$\nabla^2 \phi = 0, \quad z = \eta \tag{3.2.8}$$

The dynamic boundary condition at the free surface is as follows:

$$g\eta + \frac{\partial \phi}{\partial t} = 0, \quad z = \eta \tag{3.2.9}$$

Using Taylor series to expand (3.2.8), [23] obtained:

$$\nabla \phi^2 = 0, \quad z = 0 \tag{3.2.10}$$

Thus, equation (3.2.6) can be written as follows:

$$\frac{\partial^2 \phi}{\partial t^2} - c^2 \nabla^2 \phi + g \frac{\partial \phi}{\partial z} = 0, \qquad -h \leq z \leq 0 \tag{3.2.11}$$

In this context, H represents the freely chosen amplitude of the wave, determining the elevation of the free surface:

$$\eta = H \cos(kx - \omega t). \tag{3.2.12}$$

To find a progressive-wave solution characterized by the frequency ω, the following was obtained by Kadri, U. and Stiassnie, M. [23] after some simple manipulations:

$$\phi = \frac{igH}{2\omega} \frac{\mu \cosh[\mu(h+z)]}{\cosh(\mu h)} \mathrm{e}^{i(kx-\omega t)} \tag{3.2.13}$$

By taking the real part and making use of the dispersion relation (3.1.4), [22] showed the contribution of the AGWs to deep currents in the ocean with constant depth using the simplified 2D compressible velocity potential:

$$\phi_n = -\frac{H_n}{2} \frac{\omega}{\mu} \frac{\cosh[\mu_n(h+z)]}{\sinh(\mu_n h)} \sin(\kappa_n x - \omega t) \tag{3.2.14}$$

where subscript n is the mode's number. By taking the derivatives of (3.2.14) with respect to x and z to get the horizontal and vertical velocities respectively:

$$\phi_{n_x} = -\frac{\partial \phi_n}{\partial x} = \frac{H_n}{2}\frac{\kappa_n}{\mu_n}\frac{\omega \cosh[\mu_n(h+z)]}{\sinh(\mu_n h)}\cos(\kappa_n x - \omega t) \tag{3.2.15}$$

$$\phi_{n_z} = -\frac{\partial \phi_n}{\partial z} = \frac{H_n}{2}\frac{\omega \sinh[\mu_n(h+z)]}{\sinh(\mu_n h)}\sin(\kappa_n x - \omega t) \tag{3.2.16}$$

By integrating (3.2.15) with respect to time, the expression of the horizontal component ξ_x of the velocity can be written as:

$$\begin{aligned}\xi_x &= x_0 + \int \phi_{n_x} dt \\ &= x_0 - \frac{H_n \kappa_n}{\mu_n}\frac{\cosh[\mu_n(z+h)]}{\mu_n \sinh(\mu h)}\sin(\kappa_n x - \omega t)\end{aligned} \tag{3.2.17}$$

Likewise, by integrating (3.2.16) with respect to time, the expression of the vertical component ξ_z of the velocity can be written as:

$$\begin{aligned}\xi_z &= z_0 + \int \phi_{n_z} dt \\ &= z_0 + \frac{H_n \sinh[\mu_n(h+z)]}{\sinh(\mu_n h)}\cos(\kappa_n x - \omega t)\end{aligned} \tag{3.2.18}$$

which can be rewritten as

$$\xi_x(x,z,t) = -A\sin(\kappa_n x - \omega t) \tag{3.2.19}$$

and

$$\xi_z(x,z,t) = B\cos(\kappa_n x - \omega t) \tag{3.2.20}$$

where

$$A = \frac{H_n \kappa_n}{\mu_n}\frac{\cosh[\mu_n(z+h)]}{\mu_n \sinh(\mu h)}\sin(\kappa_n x - \omega t) \tag{3.2.21}$$

and

$$B = \frac{H_n \sinh[\mu_n(h+z)]}{\sinh(\mu_n h)}\cos(\kappa_n x - \omega t) \tag{3.2.22}$$

then

$$\left(\frac{\xi_x}{A}\right)^2 + \left(\frac{\xi_z}{B}\right)^2 = 1 \tag{3.2.23}$$

is an ellipse equation with horizontal and vertical semiaxis A and B in x and z direction respectively. For the first mode where $\mu_0 \cong \kappa_0$ is real, A and B are decreasing exponentially with depth while for the AGW modes, figure 3.3 shows the semiaxes of water particles for μ_n is imaginary and the orbital behaves periodically with depth.

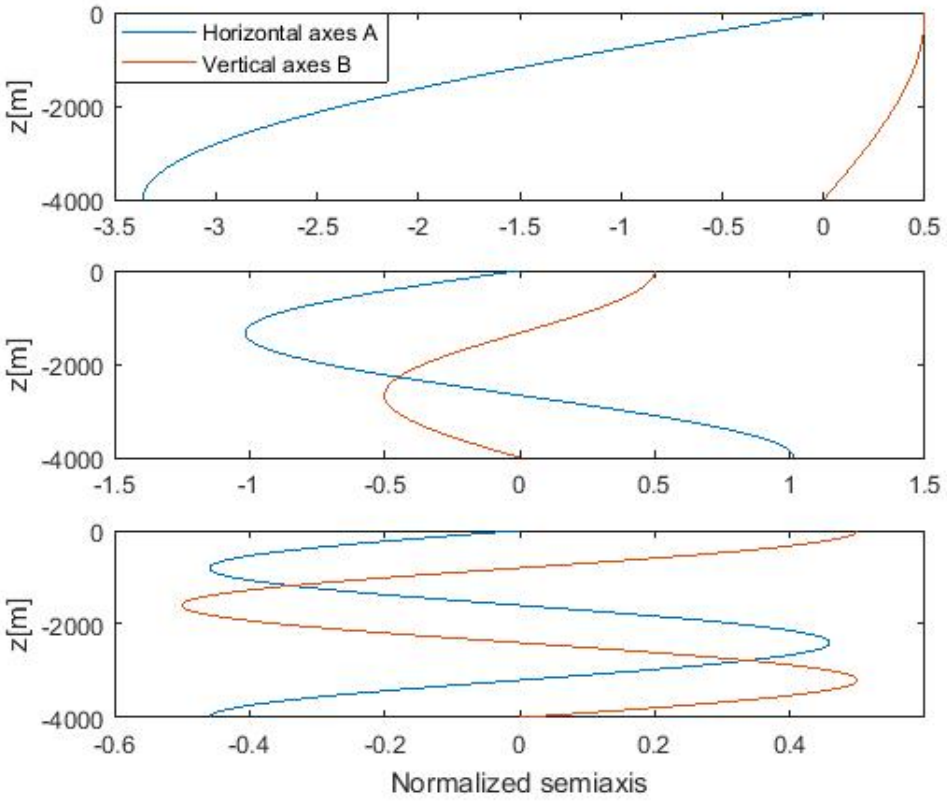

Figure 3.3: Semiaxes of water particles for AGW, with n= 1,2,3 from top to bottom

It can be shown that AGWs undergo a Stokes drift velocity in the horizontal direction where Taylor's expansion is employed to expand equation (3.2.15) around (3.2.17). The second-order partial derivative of the horizontal component ξ_x with respect to x and time is given by:

$$\frac{\partial^2 \xi_x}{\partial x \partial t} = \frac{\omega H_n \kappa_n^2}{\mu_n} \frac{\cosh[\mu_n(z+h)]}{\sinh(\mu_n h)} \sin(\kappa_n x - \omega t) \tag{3.2.24}$$

likewise, the vertical component ξ_z is expressed as follows:

$$\frac{\partial^2 \xi_z}{\partial z \partial t} = \frac{\omega H_n \kappa_n \sinh[\mu_n(z+h)]}{\sinh(\mu_n h)} \cos(k_n x - \omega t) \tag{3.2.25}$$

Thus, the Stokes drift velocity in the horizontal direction [22] is as follows:

$$\begin{aligned} D_n(x,z,t) &= (\xi_x - x)\left(\frac{\partial^2 \xi_x}{\partial x \partial t}\right) + (\xi_z - z)\left(\frac{\partial^2 \xi_z}{\partial z \partial t}\right) \\ &= \frac{\omega \kappa_n H_n^2}{4\sinh^2(\mu_n h)} \left(\frac{\kappa_n^2}{\mu_n^2} \cosh^2[\mu_n(h+z)] \sin^2(\kappa_n x - \omega t) + \sinh^2[\mu_n(h+z)] \cos^2(\kappa_n x - \omega t)\right). \end{aligned} \tag{3.2.26}$$

Figure 3.4 shows that the presence of Stokes drift is clearly observable by gravity waves near the surface (top figure), while the AGWs have contributions throughout all depths (bottom figure).

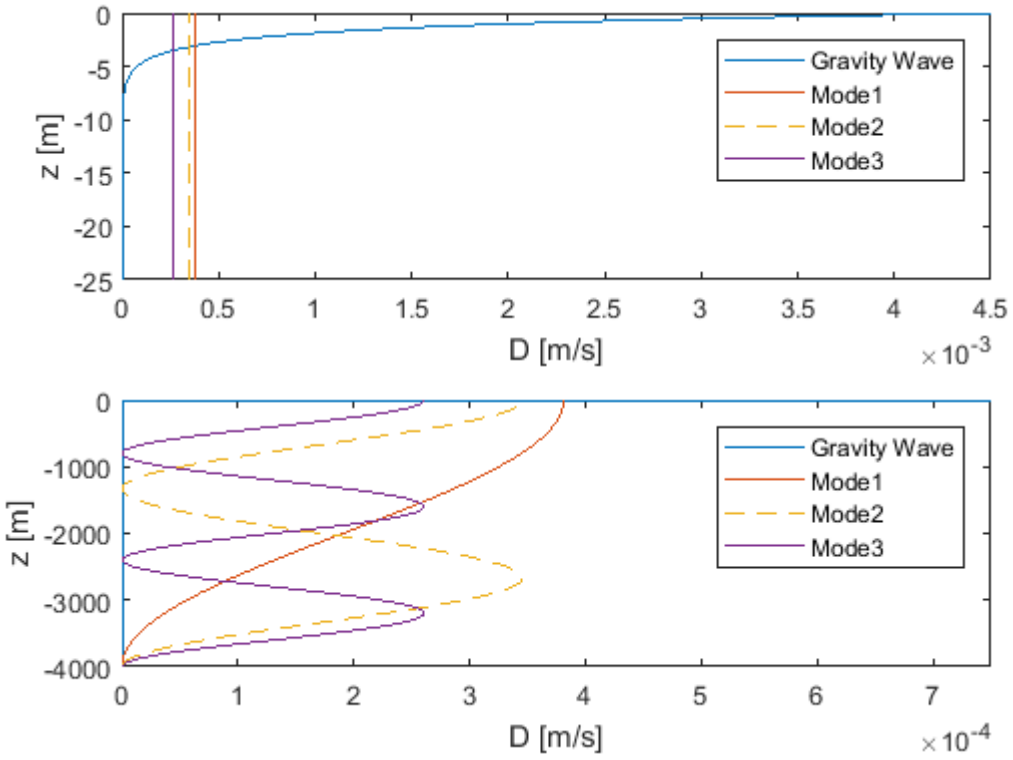

Figure 3.4: Stokes drift velocities. Gravity wave: H_1= 1.5 m, H_2= 1.5 m, σ= 2 rad/s. AGW: ω= 4 rad/s, c= 1500 m/s, h= 4000 m, g= 9.8 m/s^2.

Chapter 4

Deep water transport by AGWs generated by a slender fault - 3D approach

4.1 Modelling water drifting induced by submarine earthquakes

In this chapter, the derivation of the displacements and velocities of water particles in the x, y, and z directions due to a slender fault will be carried out benefiting from the findings in [31]. This section is dedicated to investigating the complex dynamics associated with water drifting initiated by the seismic activities of submarine earthquakes in the ocean. The primary objective is to formulate a feasible solution for describing this water drift, thus solving the underlying complexities. The predominant factor shaping flow dynamics within the fault area is the uplift mechanism. This mechanism leads to a significant elevation of the water column, rendering the influence of acoustic propagation on fluid movement negligible in this region. Consequently, the movement of fluid parcels due to acoustic waves is minimal, highlighting the dominant role of the uplift mechanism in driving flow dynamics. The foundational assumptions include an ocean depth of h= 4000 m and the recognition of slightly compressible water prop-

erties. Consequently, the flow is assumed to be irrotational, Furthermore, the impact of water viscosity is disregarded due to the prevalence of the dominant acoustic mode $\omega_1 = \pi c/2h$, resulting in the insignificance of viscosity effects. Taking the slight compressibility into account, the velocity potential follows the standard 3-D wave equation (3.1.1):

$$\left(\frac{\partial^2}{\partial x^2} + \frac{\partial^2}{\partial y^2} + \frac{\partial^2}{\partial z^2}\right)\phi = \frac{1}{c^2}\frac{\partial^2 \phi}{\partial t^2} \tag{4.1.1}$$

This includes boundary conditions that control the behaviour of the system at different interfaces. At the ocean's free surface and ignoring gravity, the equation

$$\phi = 0 \quad \text{for} \quad z = h \tag{4.1.2}$$

where at the ocean bottom, characterized by a rectangular strip with dimensions $L = O(100)$ in length and $b = O(10)$ in width, the ground motion triggered by the submarine earthquake is expressed as:

$$\frac{\partial \phi}{\partial z} = W(x, y, t), \quad |x| < b, \ |y| < L, \text{ and } z = 0. \tag{4.1.3}$$

In anticipation of understanding how waves propagate far from the seismic source, especially over distances greater than $O(1000)$, the introduction of multiple scale coordinates becomes a valuable approach. This innovative framework involves variables

$$x, y; \quad X = \epsilon^2 x \quad \text{and} \quad Y = \epsilon y \tag{4.1.4}$$

For x and X,

$$\begin{aligned} \frac{\partial \phi}{\partial x} \implies & \frac{\partial \phi}{\partial x}(x, X, Y, z, t)\frac{\partial x}{\partial x} + \frac{\partial \phi}{\partial X}(x, X, Y, z, t)\frac{\partial X}{\partial x} \\ & + \frac{\partial \phi}{\partial z}(x, X, Y, z, t)\frac{\partial Y}{\partial x} + \frac{\partial \phi}{\partial x}(x, X, Y, z, t)\frac{\partial z}{\partial x} \end{aligned} \tag{4.1.5}$$

$$\frac{\partial x}{\partial x} = 1, \quad \frac{\partial X}{\partial x} = \epsilon^2, \quad \frac{\partial Y}{\partial x} = 0, \quad \frac{\partial z}{\partial x} = 0, \quad \text{and} \quad \frac{\partial t}{\partial x} = 0, \tag{4.1.6}$$

Substituting the partial derivatives of x and X with respect to x, we obtain:

$$\frac{\partial \phi}{\partial x} = \frac{\partial \phi}{\partial x} + \epsilon^2 \frac{\partial \phi}{\partial X} \tag{4.1.7}$$

rearranging terms, we have:

$$\begin{aligned} \frac{\partial^2 \phi}{\partial x^2} \implies & \frac{\partial^2 \phi}{\partial x^2}\frac{\partial x}{\partial x} + \frac{\partial^2 \phi}{\partial X \partial x}\frac{\partial X}{\partial x} + \epsilon^2 \left(\frac{\partial^2 \phi}{\partial x \partial X}\frac{\partial x}{\partial x} + \frac{\partial^2 \phi}{\partial X^2}\frac{\partial X}{\partial x} \right) \\ & = \frac{\partial^2 \phi}{\partial x^2} + 2\epsilon^2 \frac{\partial^2 \phi}{\partial x \partial X} + \epsilon^4 \frac{\partial^2 \phi}{\partial X^2} \end{aligned} \tag{4.1.8}$$

for y and Y we have

$$\begin{aligned} \frac{\partial \phi}{\partial y} \implies & \frac{\partial \phi}{\partial Y}(x, X, Y, z, t)\frac{\partial Y}{\partial y} = \epsilon \frac{\partial \phi}{\partial y} \\ & + \frac{\partial^2 \phi}{\partial y^2} \implies \epsilon \left(\frac{\partial^2 \phi}{\partial Y^2}\frac{\partial Y}{\partial y} \right) = \epsilon^2 \frac{\partial \phi}{\partial Y^2} \end{aligned} \tag{4.1.9}$$

assembling terms leads to a more illuminating version of Equation (4.1.1), which can be rewritten as below:

$$\left(\frac{\partial^2}{\partial x^2} + 2\epsilon^2 \frac{\partial^2}{\partial x \partial X} + \epsilon^2 \frac{\partial^2}{\partial Y^2} + \frac{\partial^2}{\partial z^2} \right) \phi = \frac{1}{c^2}\frac{\partial^2 \phi}{\partial t^2}, \quad 0 < z < h. \tag{4.1.10}$$

A pivotal contribution to this endeavor is drawn from [31] where the potential ϕ_0 emerges as a centerpiece, encapsulating essential insights:

$$\phi_0 = -\frac{W_0}{\pi} \mathrm{Re} \int_{\omega_N}^{\infty} \mathrm{i}\, d\omega\, \mathrm{e}^{-\mathrm{i}\omega t} \sum_{n=1}^{N} \frac{G(k_n, \omega)}{k_n h} \frac{\sin \mu_n (h - z)}{\sin \mu_n h} \mathrm{e}^{\mathrm{i}k_n |x|} \tag{4.1.11}$$

Where

$$G(k, \omega) = \frac{4 \sin(kb) \sin(\omega T)}{k\omega} \quad \text{and} \quad \mu_n = \left(n - \frac{1}{2} \right) \frac{\pi}{h} \equiv \frac{\omega_n}{c} \quad \text{for} \quad n = 1, 2, 3, \ldots \tag{4.1.12}$$

Notably, μ_n emerges as a real zero of the equation $\cos \mu h = 0$, establishing a fundamen-

tal connection. Furthermore, k is defined as:

$$k_n = \frac{\sqrt{\omega^2 - \omega_n^2}}{c} \tag{4.1.13}$$

and is real when $\omega^2 > \omega_n^2$. This study presents the solution to the pressure represented as P:

$$P = \frac{\rho W_0}{\pi} \mathrm{Re} \int_{\omega_N}^{\infty} \omega \, d\omega \sum_{n=1}^{N} A_n \frac{G(k_n, \omega) \sin \mu(h-z)}{k_n h \sin(\mu h)} \mathrm{e}^{\mathrm{i}k_n|x| - \mathrm{i}\omega t}. \tag{4.1.14}$$

where ρ denotes density and A_n is the envelope factor:

$$\begin{aligned} A_n(k_n, X, Y) = \frac{1-\mathrm{i}}{2} \left\{ C\left(\sqrt{\frac{2}{\pi\chi}}\mathscr{Y}_+\right) + C\left(\sqrt{\frac{2}{\pi\chi}}\mathscr{Y}_-\right) \right\} \\ + \frac{1+\mathrm{i}}{2} \left\{ S\left(\sqrt{\frac{2}{\pi\chi}}\mathscr{Y}_+\right) + S\left(\sqrt{\frac{2}{\pi\chi}}\mathscr{Y}_-\right) \right\}. \end{aligned} \tag{4.1.15}$$

Which anticipates the acoustic pressure at a seabed monitoring station situated in the far-field before the arrival of a tsunami. This relies on knowing the slender fault geometry, precise geographical coordinates, eruption duration, and wave speed.

4.2 Envelope analysis of the inverse envelope equation

In this section, the inverse envelope equation as introduced in [31] will be considered. The envelope factor is given by:

$$\begin{aligned} A_n(k_n, X, Y) &= \frac{2}{\pi} \int_0^{\infty} d\gamma \cos\, \gamma Y \left\{ \frac{\sin \gamma l}{\gamma} exp(-\mathrm{i}\gamma^2 v/2) \right\} \\ &= \frac{1}{\pi} \int_0^{\infty} \frac{d\gamma}{\gamma} [\sin(\gamma(l+Y)) + \sin(\gamma(l-Y))] \, \cos(\gamma^2 \, v/2) \\ &\quad - \frac{\mathrm{i}}{\pi} \int_0^{\infty} \frac{d\gamma}{\gamma} [\sin(\gamma(l+Y)) + \sin(\gamma(l-Y))] \, \sin(\gamma^2 \, v/2) \end{aligned} \tag{4.2.16}$$

Within this framework, a key parameter emerges as $\chi = \frac{X}{2k_n}$, where $X = \epsilon^2 x$. Additionally, let:

$$\begin{aligned} 2\mathscr{Y}_+ &= l + Y \\ 2\mathscr{Y}_- &= l - Y \end{aligned} \qquad \text{with} \qquad Y = \epsilon y. \tag{4.2.17}$$

Further analysis proceeds by setting $\chi = \frac{v}{2}$, $2\mathscr{Y}_+ = l + Y$, and $2\mathscr{Y}_- = l - Y$, leading to the following results:

$$\frac{1}{2}\frac{d}{d\mathscr{Y}}\int_0^\infty \frac{d\gamma}{\gamma}\,\cos\chi\gamma^2\,\sin 2\mathscr{Y}\gamma = \int_0^\infty d\gamma\,\cos\chi\gamma^2\,\cos 2\mathscr{Y}\gamma = \frac{1}{2}\sqrt{\frac{\pi}{2\chi}}\left\{\cos\frac{\mathscr{Y}^2}{\chi} + \sin\frac{\mathscr{Y}^2}{\chi}\right\} \tag{4.2.18}$$

and

$$\frac{1}{2}\frac{d}{d\mathscr{Y}}\int_0^\infty \frac{d\gamma}{\gamma}\,\sin\chi\gamma^2\,\sin 2\mathscr{Y}\gamma = \int_0^\infty d\gamma\,\sin\chi\gamma^2\,\cos 2\mathscr{Y}\gamma = \frac{1}{2}\sqrt{\frac{\pi}{2\chi}}\left\{\cos\frac{\mathscr{Y}^2}{\chi} - \sin\frac{\mathscr{Y}^2}{\chi}\right\} \tag{4.2.19}$$

These expressions, after employing integral formulas from [18], can be written more simply as:

$$\begin{aligned} \frac{1}{2}\frac{d}{d\mathscr{Y}}\int_0^\infty \frac{d\gamma}{\gamma}\,\cos\chi\gamma^2\,\sin 2\mathscr{Y}\gamma &= \int_0^{\mathscr{Y}} d\mathscr{Y}\sqrt{\frac{\pi}{2\chi}}\left\{\cos\frac{\mathscr{Y}^2}{\chi} + \sin\frac{\mathscr{Y}^2}{\chi}\right\} \\ &= \frac{\pi}{2}\left\{C\left(\sqrt{\frac{2}{\pi\chi}}\mathscr{Y}\right) + S\left(\sqrt{\frac{2}{\pi\chi}}\mathscr{Y}\right)\right\} \end{aligned} \tag{4.2.20}$$

and

$$\begin{aligned} \frac{1}{2}\frac{d}{d\mathscr{Y}}\int_0^\infty \frac{d\gamma}{\gamma}\,\sin\chi\gamma^2\,\sin 2\mathscr{Y}\gamma &= \int_0^{\mathscr{Y}} d\mathscr{Y}\sqrt{\frac{\pi}{2\chi}}\left\{\cos\frac{\mathscr{Y}^2}{\chi} - \sin\frac{\mathscr{Y}^2}{\chi}\right\} \\ &= \frac{\pi}{2}\left\{C\left(\sqrt{\frac{2}{\pi\chi}}\mathscr{Y}\right) - S\left(\sqrt{\frac{2}{\pi\chi}}\mathscr{Y}\right)\right\} \end{aligned} \tag{4.2.21}$$

In these equations, $C(f)$ and $S(f)$ represent Fresnel integrals [4].This thorough anal-

ysis concludes with the development of the envelope factor for mode n:

$$\begin{aligned} A_n(k_n,X,Y) = \frac{1-\mathrm{i}}{2}\left\{C\left(\sqrt{\frac{2}{\pi\chi}}\mathscr{Y}_+\right)+C\left(\sqrt{\frac{2}{\pi\chi}}\mathscr{Y}_-\right)\right\} \\ +\frac{1+\mathrm{i}}{2}\left\{S\left(\sqrt{\frac{2}{\pi\chi}}\mathscr{Y}_+\right)+S\left(\sqrt{\frac{2}{\pi\chi}}\mathscr{Y}_-\right)\right\} \end{aligned} \tag{4.2.22}$$

4.3 Derivatives of the envelope factor

In this section, the derivatives of the envelope factor to obtain velocities and displacements will be carried out. The envelope factor is an important component in wave propagation analyses as it captures the overall shape and behavior of a wave packet, including changes in amplitude over time. By incorporating effects like dispersion and attenuation, it provides a more accurate representation of wave propagation. Beginning by introducing the Fresnel integrals and their derivatives, which play a fundamental role in the subsequent derivations.

Fresnel integrals and their derivatives

Fresnel integrals, $C(x)$ and $S(x)$, are defined as follows [4]:

$$\begin{aligned} C(f) &= \int_0^f \cos\left(\frac{\pi}{2}t^2\right)dt \\ S(f) &= \int_0^f \sin\left(\frac{\pi}{2}t^2\right)dt \end{aligned} \tag{4.3.23}$$

where in this study $f = \sqrt{\frac{2}{\pi\chi}}\mathscr{Y}$. Their derivatives with respect to their arguments are given by:

$$\begin{aligned} \frac{\partial C}{\partial f} &= \cos\left(\frac{\pi}{2}f^2\right), \\ \frac{\partial S}{\partial f} &= \sin\left(\frac{\pi}{2}f^2\right). \end{aligned} \tag{4.3.24}$$

differentiating f with respect to χ and $\mathscr{Y}$, to get:

$$\begin{aligned}\frac{\partial f}{\partial \chi} &= -\frac{1}{2}\sqrt{\frac{2}{\pi\chi^3}}\,\mathscr{Y}_{\pm},\\ \frac{\partial f}{\partial \mathscr{Y}_{\pm}} &= \sqrt{\frac{2}{\pi\chi}}.\end{aligned} \tag{4.3.25}$$

where

$$\frac{\partial \chi}{\partial X} = \frac{1}{2k_n}, \quad \frac{\partial X}{\partial x} = \epsilon^2, \quad \frac{\partial \mathscr{Y}_{+}}{\partial Y} = \frac{1}{2}, \quad \frac{\partial \mathscr{Y}_{-}}{\partial Y} = -\frac{1}{2}, \quad and \quad \frac{\partial Y}{\partial y} = \epsilon. \tag{4.3.26}$$

Beginning by differentiating $C(f)$ with respect to x and y:

$$\frac{\partial C}{\partial x} = -\frac{\epsilon^2}{4k_n}\sqrt{\frac{2}{\pi\chi^3}}\mathscr{Y}_{\pm}\cos\left(\frac{\mathscr{Y}_{\pm}^2}{\chi}\right) \tag{4.3.27}$$

and

$$\frac{\partial C}{\partial y} = \pm\frac{\epsilon}{2}\sqrt{\frac{2}{\pi\chi}}\cos\left(\frac{\mathscr{Y}_{\pm}^2}{\chi}\right) \tag{4.3.28}$$

These derivatives are computed based on equations (4.3.24), (4.3.25), and (4.3.26).

Similarly, differentiating $S(f)$ with respect to x and y:

$$\frac{\partial S}{\partial x} = -\frac{\epsilon^2}{4k_n}\sqrt{\frac{2}{\pi\chi^3}}\mathscr{Y}_{\pm}\sin\left(\frac{\mathscr{Y}_{\pm}^2}{\chi}\right) \tag{4.3.29}$$

and

$$\frac{\partial S}{\partial y} = \pm\frac{\epsilon}{2}\sqrt{\frac{2}{\pi\chi}}\sin\left(\frac{\mathscr{Y}_{\pm}^2}{\chi}\right) \tag{4.3.30}$$

Differentiation of the envelope factor

Now, putting everything together and implementing differentiation of the envelope factor An with respect to x and y.

starting with the derivatives of the envelope factor with respect to (x):

$$\begin{aligned} A_{n_x} = \frac{\mathrm{i}-1}{2}\left\{\frac{\epsilon^2}{4k_n}\sqrt{\frac{2}{\pi\chi^3}}\mathscr{Y}_+\cos\left(\frac{\mathscr{Y}_+^2}{\chi}\right)+\frac{\epsilon^2}{4k_n}\sqrt{\frac{2}{\pi\chi^3}}\mathscr{Y}_-\cos\left(\frac{\mathscr{Y}_-^2}{\chi}\right)\right\} \\ -\left(\frac{1+\mathrm{i}}{2}\right)\left\{\frac{\epsilon^2}{4k_n}\sqrt{\frac{2}{\pi\chi^3}}\mathscr{Y}_+\sin\left(\frac{\mathscr{Y}_+^2}{\chi}\right)+\frac{\epsilon^2}{4k_n}\sqrt{\frac{2}{\pi\chi^3}}\mathscr{Y}_-\sin\left(\frac{\mathscr{Y}_-^2}{\chi}\right)\right\} \end{aligned} \tag{4.3.31}$$

then with respect to (y)

$$\begin{aligned} A_{n_y} = \frac{1-\mathrm{i}}{2}\left\{\frac{\epsilon}{2}\sqrt{\frac{2}{\pi\chi}}\cos\left(\frac{\mathscr{Y}_+^2}{\chi}\right)-\frac{\epsilon}{2}\sqrt{\frac{2}{\pi\chi}}\cos\left(\frac{\mathscr{Y}_-^2}{\chi}\right)\right\} \\ +\frac{1+\mathrm{i}}{2}\left\{\frac{\epsilon}{2}\sqrt{\frac{2}{\pi\chi}}\sin\left(\frac{\mathscr{Y}_+^2}{\chi}\right)-\frac{\epsilon}{2}\sqrt{\frac{2}{\pi\chi}}\sin\left(\frac{\mathscr{Y}_-^2}{\chi}\right)\right\} \end{aligned} \tag{4.3.32}$$

For simplicity and verification, and starting by differentiating the envelope factor with respect to y, while taking into account equations (4.2.20) and (4.2.21), which can be substituted into equation (4.2.16):

$$\begin{aligned} A_n = &\frac{1}{\pi}\left(\int_0^{\mathscr{Y}_+} d\mathscr{Y}_+\sqrt{\frac{\pi}{2\chi}}\left\{\cos\frac{\mathscr{Y}_+^2}{\chi}+\sin\frac{\mathscr{Y}_+^2}{\chi}\right\}+\int_0^{\mathscr{Y}_-} d\mathscr{Y}_-\sqrt{\frac{\pi}{2\chi}}\left\{\cos\frac{\mathscr{Y}_-^2}{\chi}+\sin\frac{\mathscr{Y}_-^2}{\chi}\right\}\right) \\ &-\frac{\mathrm{i}}{\pi}\left(\int_0^{\mathscr{Y}_+} d\mathscr{Y}_+\sqrt{\frac{\pi}{2\chi}}\left\{\cos\frac{\mathscr{Y}_+^2}{\chi}-\sin\frac{\mathscr{Y}_+^2}{\chi}\right\}+\int_0^{\mathscr{Y}_-} d\mathscr{Y}_-\sqrt{\frac{\pi}{2\chi}}\left\{\cos\frac{\mathscr{Y}_-^2}{\chi}-\sin\frac{\mathscr{Y}_-^2}{\chi}\right\}\right) \end{aligned} \tag{4.3.33}$$

The differentiation of equation (4.3.33) with respect to y is as follows:

$$\frac{dA_n}{dy} = \frac{dA_n}{d\mathscr{Y}}\frac{d\mathscr{Y}}{dY}\frac{dY}{dy} \tag{4.3.34}$$

$$\begin{aligned} \frac{dA_n}{d\mathscr{Y}} = &\frac{1}{\pi}\left(\sqrt{\frac{\pi}{2\chi}}\left\{\cos\frac{\mathscr{Y}_+^2}{\chi}+\sin\frac{\mathscr{Y}_+^2}{\chi}\right\}+\sqrt{\frac{\pi}{2\chi}}\left\{\cos\frac{\mathscr{Y}_-^2}{\chi}+\sin\frac{\mathscr{Y}_-^2}{\chi}\right\}\right) \\ &-\frac{\mathrm{i}}{\pi}\left(\sqrt{\frac{\pi}{2\chi}}\left\{\cos\frac{\mathscr{Y}_+^2}{\chi}-\sin\frac{\mathscr{Y}_+^2}{\chi}\right\}+\sqrt{\frac{\pi}{2\chi}}\left\{\cos\frac{\mathscr{Y}_-^2}{\chi}-\sin\frac{\mathscr{Y}_-^2}{\chi}\right\}\right) \end{aligned} \tag{4.3.35}$$

rearranging and simplifying to get:

$$\begin{aligned}\frac{dA_n}{d\mathscr{Y}} =&(1-\mathrm{i})\left(\sqrt{\frac{1}{2\pi\chi}}\cos\left(\frac{\mathscr{Y}_+^2}{\chi}\right)+\sqrt{\frac{1}{2\pi\chi}}\cos\left(\frac{\mathscr{Y}_-^2}{\chi}\right)\right)\\ &+(1+\mathrm{i})\left(\sqrt{\frac{1}{2\pi\chi}}\sin\left(\frac{\mathscr{Y}_+^2}{\chi}\right)+\sqrt{\frac{1}{2\pi\chi}}\sin\left(\frac{\mathscr{Y}_-^2}{\chi}\right)\right)\end{aligned} \tag{4.3.36}$$

using (4.3.26) to get:

$$\begin{aligned}\frac{dA_n}{dy} =&\frac{1-\mathrm{i}}{2}\left(\epsilon\sqrt{\frac{1}{2\pi\chi}}\cos\left(\frac{\mathscr{Y}_+^2}{\chi}\right)-\epsilon\sqrt{\frac{1}{2\pi\chi}}\cos\left(\frac{\mathscr{Y}_-^2}{\chi}\right)\right)\\ &+\frac{1+\mathrm{i}}{2}\left(\epsilon\sqrt{\frac{1}{2\pi\chi}}\sin\left(\frac{\mathscr{Y}_+^2}{\chi}\right)-\epsilon\sqrt{\frac{1}{2\pi\chi}}\sin\left(\frac{\mathscr{Y}_-^2}{\chi}\right)\right)\end{aligned} \tag{4.3.37}$$

Hence, this expression verifies equation (4.3.32).

Continuing, the second partial derivative $A_{n_{xx}}$ is given by:

$$\begin{aligned}A_{n_{xx}} =&\frac{\mathrm{i}-1}{2}\left[\frac{-3\epsilon^4\mathscr{Y}_+}{16k_n^2}\sqrt{\frac{2}{\pi\chi^5}}\cos\left(\frac{\mathscr{Y}_+^2}{\chi}\right)+\frac{\epsilon^4\mathscr{Y}_+^3}{8k_n^2\chi^2}\sqrt{\frac{2}{\pi\chi^3}}\sin\left(\frac{\mathscr{Y}_+^2}{\chi}\right)\right.\\ &\left.-\frac{3\epsilon^4\mathscr{Y}_-}{16k_n^2}\sqrt{\frac{2}{\pi\chi^5}}\cos\left(\frac{\mathscr{Y}_-^2}{\chi}\right)+\frac{\epsilon^4\mathscr{Y}_-^3}{8k_n^2\chi^2}\sqrt{\frac{2}{\pi\chi^3}}\sin\left(\frac{\mathscr{Y}_-^2}{\chi}\right)\right]\\ &-\left(\frac{1+\mathrm{i}}{2}\right)\left[\frac{-3\epsilon^4\mathscr{Y}_+}{16k_n^2}\sqrt{\frac{2}{\pi\chi^5}}\sin\left(\frac{\mathscr{Y}_+^2}{\chi}\right)-\frac{\epsilon^4\mathscr{Y}_+^3}{8k_n^2\chi^2}\sqrt{\frac{2}{\pi\chi^3}}\cos\left(\frac{\mathscr{Y}_+^2}{\chi}\right)\right.\\ &\left.-\frac{3\epsilon^4\mathscr{Y}_-}{16k_n^2}\sqrt{\frac{2}{\pi\chi^5}}\sin\left(\frac{\mathscr{Y}_-^2}{\chi}\right)+\frac{\epsilon^4\mathscr{Y}_-^3}{8k_n^2\chi^2}\sqrt{\frac{2}{\pi\chi^3}}\cos\left(\frac{\mathscr{Y}_-^2}{\chi}\right)\right]\end{aligned} \tag{4.3.38}$$

The partial derivative $A_{n_{xy}}$ is expressed as:

$$
\begin{aligned}
A_{n_{xy}} = \frac{\mathrm{i}-1}{2}\Bigg[& \frac{\epsilon^3}{8k_n}\sqrt{\frac{2}{\pi\chi^3}}\cos\left(\frac{\mathscr{Y}_+^2}{\chi}\right) - \frac{\epsilon^3\mathscr{Y}_+^2}{4k_n\chi}\sqrt{\frac{2}{\pi\chi^3}}\sin\left(\frac{\mathscr{Y}_+^2}{\chi}\right) \\
& - \frac{\epsilon^3}{8k_n}\sqrt{\frac{2}{\pi\chi^3}}\cos\left(\frac{\mathscr{Y}_-^2}{\chi}\right) + \frac{\epsilon^3\mathscr{Y}_-^2}{4k_n\chi}\sqrt{\frac{2}{\pi\chi^3}}\sin\left(\frac{\mathscr{Y}_-^2}{\chi}\right)\Bigg] \\
& - \left(\frac{1+\mathrm{i}}{2}\right)\Bigg[\frac{\epsilon^3}{8k_n}\sqrt{\frac{2}{\pi\chi^3}}\sin\left(\frac{\mathscr{Y}_+^2}{\chi}\right) + \frac{\epsilon^3\mathscr{Y}_+^2}{4k_n\chi}\sqrt{\frac{2}{\pi\chi^3}}\cos\left(\frac{\mathscr{Y}_+^2}{\chi}\right) \\
& - \frac{\epsilon^3}{8k_n}\sqrt{\frac{2}{\pi\chi^3}}\sin\left(\frac{\mathscr{Y}_-^2}{\chi}\right) + \frac{\epsilon^3\mathscr{Y}_-^2}{4k_n\chi}\sqrt{\frac{2}{\pi\chi^3}}\cos\left(\frac{\mathscr{Y}_-^2}{\chi}\right)\Bigg]
\end{aligned}
\tag{4.3.39}
$$

Moving forward, the second partial derivative $A_{n_{yy}}$ is computed as:

$$
\begin{aligned}
A_{n_{yy}} = & \frac{1-\mathrm{i}}{2}\left\{\frac{-\epsilon^3\mathscr{Y}_+}{2\chi}\sqrt{\frac{2}{\pi\chi}}\sin\left(\frac{\mathscr{Y}_+^2}{\chi}\right) - \frac{\epsilon^2\mathscr{Y}_-}{2\chi}\sqrt{\frac{2}{\pi\chi}}\sin\left(\frac{\mathscr{Y}_-^2}{\chi}\right)\right\} \\
& + \left(\frac{1-\mathrm{i}}{2}\right)\left\{\frac{\epsilon^2\mathscr{Y}_+}{2\chi}\sqrt{\frac{2}{\pi\chi}}\cos\left(\left(\frac{\mathscr{Y}_+^2}{\chi}\right) + \frac{\epsilon^2\mathscr{Y}_-}{2\chi}\sqrt{\frac{2}{\pi\chi}}\cos\left(\frac{\mathscr{Y}_-^2}{\chi}\right)\right\}\right.
\end{aligned}
\tag{4.3.40}
$$

Lastly, the partial derivative $A_{n_{yx}}$ is determined by:

$$
\begin{aligned}
A_{n_{yx}} = \frac{1-\mathrm{i}}{2}\Bigg[& \frac{-\epsilon^3}{8k_n}\sqrt{\frac{2}{\pi\chi^3}}\cos\left(\frac{\mathscr{Y}_+^2}{\chi}\right) + \frac{\epsilon^3\mathscr{Y}_+^2}{4k_n\chi^2}\sqrt{\frac{2}{\pi\chi}}\sin\left(\frac{\mathscr{Y}_+^2}{\chi}\right) \\
& + \frac{\epsilon^3}{8k_n}\sqrt{\frac{2}{\pi\chi^3}}\cos\left(\frac{\mathscr{Y}_-^2}{\chi}\right) - \frac{\epsilon^3\mathscr{Y}_-^2}{4k_n\chi^2}\sqrt{\frac{2}{\pi\chi}}\sin\left(\frac{\mathscr{Y}_-^2}{\chi}\right)\Bigg] \\
& + \left(\frac{1+\mathrm{i}}{2}\right)\Bigg[\frac{-\epsilon^3}{8k_n}\sqrt{\frac{2}{\pi\chi^3}}\sin\left(\frac{\mathscr{Y}_+^2}{\chi}\right) - \frac{\epsilon^3\mathscr{Y}_+^2}{4k_n\chi^2}\sqrt{\frac{2}{\pi\chi}}\cos\left(\frac{\mathscr{Y}_+^2}{\chi}\right) \\
& + \frac{\epsilon^3}{8k_n}\sqrt{\frac{2}{\pi\chi^3}}\sin\left(\frac{\mathscr{Y}_-^2}{\chi}\right) - \frac{\epsilon^3\mathscr{Y}_-^2}{4k_n\chi^2}\sqrt{\frac{2}{\pi\chi}}\cos\left(\frac{\mathscr{Y}_-^2}{\chi}\right)\Bigg]
\end{aligned}
\tag{4.3.41}
$$

Obtaining velocities and displacements

In this section, the derivation of velocities and displacements for the propagating part of the potential will be carried out, represented by the equation:

$$\phi_0 = -\frac{W_0}{\pi}\mathrm{Re}\int_{\omega_N}^{\infty} \mathrm{i}\, d\omega \sum_{1}^{N} A_n \frac{G(k_n,\omega)}{k_n h}\frac{\sin\mu_n(h-z)}{\sin\mu_n h}\mathrm{e}^{ik_n|x|-\mathrm{i}\omega t} \tag{4.3.42}$$

The goal is to determine the velocities and displacements associated with this potential. The derivatives of ϕ_0 with respect to x, y, and z yield the velocities while integrating the velocities with respect to time gives the displacements. The expressions for the velocities and displacements are derived as follows:

Velocities

Differentiating ϕ_0 with respect to x, y, and z, to obtain:

$$\frac{\partial\phi_0}{\partial x} = -\frac{W_0}{\pi}\mathrm{Re}\int_{\omega_N}^{\infty} \mathrm{i}\, d\omega \sum_{1}^{N} \frac{G(k_n,\omega)}{k_n h}\frac{\sin\mu_n(h-z)}{\sin\mu_n h}\mathrm{e}^{ik_n|x|-\mathrm{i}\omega t}\,(A_{n_x} + ik_n A_n) \tag{4.3.43}$$

$$\frac{\partial\phi_0}{\partial y} = -\frac{W_0}{\pi}\mathrm{Re}\int_{\omega_N}^{\infty} \mathrm{i}\, d\omega \sum_{1}^{N} A_{n_y}\frac{G(k_n,\omega)}{k_n h}\frac{\sin\mu_n(h-z)}{\sin\mu_n h}\mathrm{e}^{ik_n|x|-\mathrm{i}\omega t} \tag{4.3.44}$$

$$\frac{\partial\phi_0}{\partial z} = \frac{W_0}{\pi}\mathrm{Re}\int_{\omega_N}^{\infty} \mathrm{i}\, d\omega \sum_{1}^{N} A_n\mu_n\frac{G(k_n,\omega)}{k_n h}\frac{\cos\mu_n(h-z)}{\sin\mu_n h}\mathrm{e}^{ik_n|x|-\mathrm{i}\omega t} \tag{4.3.45}$$

Displacements

The displacement components α_n, β_n, and γ_n are obtained by integrating the corresponding velocities with respect to time:

$$\alpha_n = x_0 - \frac{W_0}{\mathrm{i}\omega\pi}\,\mathrm{Re}\int_{\omega_N}^{\infty}\mathrm{i}\,d\omega\sum_{1}^{N}\frac{G(k_n,\omega)}{k_n h}\frac{\sin\mu_n(h-z)}{\sin\mu_n h}\mathrm{e}^{ik_n|x|-\mathrm{i}\omega t}\,(\epsilon^2 A_{n_x}+ik_n A_n) \tag{4.3.46}$$

$$\beta_n = y_0 - \frac{\epsilon W_0}{\mathrm{i}\omega\pi}\,\mathrm{Re}\int_{\omega_N}^{\infty}\mathrm{i}\,d\omega\sum_{1}^{N}A_{n_y}\frac{G(k_n,\omega)}{k_n h}\frac{\sin\mu_n(h-z)}{\sin\mu_n h}\mathrm{e}^{ik_n|x|-\mathrm{i}\omega t} \tag{4.3.47}$$

$$\gamma_n = z_0 + \frac{W_0}{\mathrm{i}\omega\pi}\,\mathrm{Re}\int_{\omega_N}^{\infty}\mathrm{i}\,d\omega\sum_{1}^{N}A_n\mu_n\frac{G(k_n,\omega)}{k_n h}\frac{\cos\mu_n(h-z)}{\sin\mu_n h}\mathrm{e}^{ik_n|x|-\mathrm{i}\omega t} \tag{4.3.48}$$

These derived equations provide insights into the velocities and displacements associated with the potential ϕ_0, contributing to a comprehensive understanding of wave propagation in various physical contexts.

4.4 Stationary-phase approximation for large t

In this section, the stationary-phase approximation for the propagation part of the potential will be employed, which will be applied to the velocities and displacements [51]. The potential is given by the integral

$$\phi_0 = -\frac{W_0}{\pi}\,\mathrm{Re}\int_{\omega_N}^{\infty}\mathrm{i}\,d\omega\sum_{1}^{N}A_n\frac{G(k_n,\omega)}{k_n h}\frac{\sin\mu_n(h-z)}{\sin\mu_n h}\mathrm{e}^{ik_n|x|-\mathrm{i}\omega t} \tag{4.4.49}$$

for large t, with fixed x/ct and $x>0$. Here, the phase of mode n is denoted by $g_n(\omega)$

$$g_n(\omega) = k_n\frac{x}{t} - \omega, \quad \text{where} \quad k_n(\omega) = \frac{\sqrt{\omega^2-\omega_n^2}}{c}. \tag{4.4.50}$$

This phase $g_n(\omega)$ is such that

$$\frac{\partial g_n}{\partial \omega} = \frac{\omega}{\sqrt{\omega^2 - \omega_n^2}} \frac{x}{ct} - 1 \tag{4.4.51}$$

The stationary phase point is located at $\Omega_n = \omega$, where $\frac{\partial g_n}{\partial \omega} = 0$. Thus,

$$\frac{\Omega_n}{\sqrt{\Omega_n^2 - \omega_n^2}} = \frac{ct}{x} \tag{4.4.52}$$

leading to

$$\Omega_n = \frac{\omega_n}{\sqrt{1 - (x/ct)^2}} \tag{4.4.53}$$

and

$$\Omega_n^2 - \omega_n^2 = \omega_n^2 \left(\frac{1}{1 - (x/ct)^2} - 1 \right) = \omega_n^2 \frac{(x/ct)^2}{1 - (x/ct)^2} \tag{4.4.54}$$

where $\Omega_n > \omega_n$. differentiating 4.4.51, to get

$$\begin{aligned} \frac{\partial^2 g}{\partial \omega^2} &= \frac{x}{ct} \left(\frac{1}{\sqrt{\Omega_n^2 - \omega_n^2}} - \frac{\omega^2}{(\Omega_n^2 - \omega_n^2)^{3/2}} \right) \\ &= \frac{x}{ct} \frac{\omega^2 - \omega_n^2 - \omega^2}{(\Omega_n^2 - \omega_n^2)^{3/2}} = \frac{-\omega_n^2 (x/ct)}{(\Omega_n^2 - \omega_n^2)^{3/2}} < 0 \end{aligned} \tag{4.4.55}$$

At the stationary phase point

$$k_n(\Omega_n) \equiv K_n = \frac{1}{c} \sqrt{\Omega_n^2 - \omega_n^2} = \frac{\omega_n}{c} \frac{x/ct}{\sqrt{1 - (x/ct)^2}} \tag{4.4.56}$$

Using the stationary phase approximation, the potential becomes

$$\begin{aligned}\phi &= \frac{W_0}{\pi}\,\mathrm{Re}\sum_1^N \mathrm{i}An(K_n,X,Y)\mathrm{i}\frac{G(K_n,\Omega_n)}{K_n h}\frac{\sin\mu_n(h-z)}{\sin\mu_n h}\left[\frac{2\pi}{t\frac{x}{ct}(\Omega_n^2-\omega_n^2)^{3/2}}\right]^{1/2} \mathrm{e}^{\mathrm{i}(k_n|x|-\Omega_n t-\pi/4)} \\ &= \frac{W_0}{\pi}\,\mathrm{Re}\sum_1^N \mathrm{i}A_n(K_n,X,Y)\frac{G(K_n,\Omega_n)}{K_n h}\left[\frac{2\pi}{\frac{x}{c}\frac{\omega_n^2}{(\Omega_n^2-\omega_n^2)^{3/2}}}\right]^{1/2} \frac{\sin\mu_n(h-z)}{\sin\mu_n h} \\ &\quad\times \mathrm{e}^{\mathrm{i}(k_n|x|-\Omega_n t-\pi/4)}\end{aligned} \tag{4.4.57}$$

where ψ_n^A represents the phase of the complex A.

Now, introducing the definition

$$\phi = \mathrm{Re}\sum_1^N \phi_n\,\mathrm{e}^{\mathrm{i}(K_n x-\Omega_n t-\frac{\pi}{4})} \tag{4.4.58}$$

Hence, ϕ_n represents the potential of mode n:

$$\begin{aligned}\phi_n &= \mathrm{Re}\frac{\mathrm{i}W_0}{\pi}A_n(K_n,X,Y)\frac{G(K_n,\Omega_n)}{h/c}\sqrt{\frac{2\pi c}{x\omega_n^2}}\frac{\sin\mu_n(h-z)}{\sin\mu_n h}\frac{(\Omega_n^2-\omega_n^2)^{3/4}}{(\Omega_n^2-\omega_n^2)^{1/2}} \\ &= \mathrm{Re}\frac{\mathrm{i}W_0}{\pi}A_n(K_n,X,Y)\frac{G(K_n,\Omega_n)}{h/c}\sqrt{\frac{2\pi c}{x}}\frac{\sin\mu_n(h-z)}{\sin\mu_n h}\frac{(\Omega_n^2-\omega_n^2)^{1/4}}{\omega_n} \\ &= \mathrm{Re}\frac{\mathrm{i}W_0}{\pi}A_n(K_n,X,Y)\frac{G(K_n,\Omega_n)}{h/c}\sqrt{\frac{2\pi c}{x}}\frac{\sin\mu_n(h-z)}{\sin\mu_n h}\frac{(\frac{x}{ct})^{1/2}}{\omega_n^{1/2}\left(1-(\frac{x}{ct})^2\right)^{1/4}}\end{aligned} \tag{4.4.59}$$

since

$$G(K_n,\Omega_n) = \frac{4\sin(K_n b)\sin(\Omega_n\tau)}{K_n\Omega_n} = \frac{4\sin\left(\frac{\omega_n}{c}\frac{x/ct}{\sqrt{1-(x/ct)^2}}b\right)\sin\left(\frac{\omega_n}{\sqrt{1-(x/ct)^2}}\tau\right)}{\frac{\omega_n}{c}\frac{x/ct}{\sqrt{1-(x/ct)^2}}\frac{\omega_n}{\sqrt{1-(x/ct)^2}}} \tag{4.4.60}$$

we have

$$\phi_n = \mathrm{Re}\frac{iW_0}{\pi}\frac{A_n}{h/c}\frac{4\sin\left(\frac{\omega_n}{c}\frac{x/ct}{\sqrt{1-(x/ct)^2}}b\right)\sin\left(\frac{\omega_n}{\sqrt{1-(x/ct)^2}}\tau\right)}{\frac{\omega_n}{c}\frac{x/ct}{\sqrt{1-(x/ct)^2}}\frac{\omega_n}{\sqrt{1-(x/ct)^2}}}\sqrt{\frac{2\pi c}{x}}$$
$$\frac{\sin\mu_n(h-z)}{\sin\mu_n h}\frac{(x/ct)^{1/2}}{\omega_n^{1/2}\left(1-(\frac{x}{ct})^2\right)^{1/4}}$$
$$= \mathrm{Re}\frac{\mathrm{i}W_0A_n}{h\pi^{1/2}}\frac{2^{5/2}c^3t^{1/2}}{\omega_n^{5/2}x}[1-(x/ct)^2]^{3/4}\sin\left(\frac{\omega_n}{c}\frac{x/ct}{\sqrt{1-(x/ct)^2}}b\right)\sin\left(\frac{\omega_n}{\sqrt{1-(x/ct)^2}}\tau\right)$$
$$\frac{\sin\mu_n(h-z)}{\sin\mu_n h} \tag{4.4.61}$$

Applying the stationary phase approximation to the velocities, to have

$$\phi_x = -\mathrm{Re}\sum_0^N \mathrm{i}W_0\frac{2^{5/2}c^3t^{1/2}}{h\pi^{1/2}\omega_n^{5/2}x}[1-(x/ct)^2]^{3/4}\sin\left(\frac{\omega_n}{c}\frac{x/ct}{\sqrt{1-(x/ct)^2}}b\right)\sin\left(\frac{\omega_n}{\sqrt{1-(x/ct)^2}}\tau\right)$$
$$\frac{\sin\mu_n(h-z)}{\sin\mu_n h}\left(A_{n_x}+ik_nA_n\right)\mathrm{e}^{\mathrm{i}(K_nx-\Omega_nt-\frac{\pi}{4})} \tag{4.4.62}$$

$$\phi_y = -\mathrm{Re}\sum_0^N \mathrm{i}W_0\frac{2^{5/2}c^3t^{1/2}}{h\pi^{1/2}\omega_n^{5/2}x}[1-(x/ct)^2]^{3/4}\sin\left(\frac{\omega_n}{c}\frac{x/ct}{\sqrt{1-(x/ct)^2}}b\right)\sin\left(\frac{\omega_n}{\sqrt{1-(x/ct)^2}}\tau\right)$$
$$\frac{\sin\mu_n(h-z)}{\sin\mu_n h}A_{n_y}\mathrm{e}^{\mathrm{i}(K_nx-\Omega_nt-\frac{\pi}{4})} \tag{4.4.63}$$

$$\phi_z = \mathrm{Re}\sum_0^N \mathrm{i}W_0\frac{2^{5/2}c^3t^{1/2}}{h\pi^{1/2}\omega_n^{5/2}x}[1-(x/ct)^2]^{3/4}\sin\left(\frac{\omega_n}{c}\frac{x/ct}{\sqrt{1-(x/ct)^2}}b\right)\sin\left(\frac{\omega_n}{\sqrt{1-(x/ct)^2}}\tau\right)$$
$$\frac{\cos\mu_n(h-z)}{\sin\mu_n h}A_n\mu_n\mathrm{e}^{\mathrm{i}(K_nx-\Omega_nt-\frac{\pi}{4})} \tag{4.4.64}$$

Applying the stationary phase approximation to the displacements, to obtain

$$\alpha_n = x_0 - \mathrm{Re}\sum_0^N W_0 \frac{2^{5/2} c^3 t^{1/2}}{h\pi^{1/2}\omega_n^{7/2} x}[1-(x/ct)^2]^{3/4} \sin\left(\frac{\omega_n}{c}\frac{x/ct}{\sqrt{1-(x/ct)^2}}b\right)\sin\left(\frac{\omega_n}{\sqrt{1-(x/ct)^2}}\tau\right) \frac{\sin\mu_n(h-z)}{\sin\mu_n h}\left(A_{n_x} + ik_n A_n\right)\mathrm{e}^{\mathrm{i}(K_n x - \Omega_n t - \frac{\pi}{4})} \tag{4.4.65}$$

$$\beta_n = y - \mathrm{Re}\sum_0^N W_0 \frac{2^{5/2} c^3 t^{1/2}}{h\pi^{1/2}\omega_n^{7/2} x}[1-(x/ct)^2]^{3/4} \sin\left(\frac{\omega_n}{c}\frac{x/ct}{\sqrt{1-(x/ct)^2}}b\right)\sin\left(\frac{\omega_n}{\sqrt{1-(x/ct)^2}}\tau\right) \frac{\sin\mu_n(h-z)}{\sin\mu_n h} A_{n_y}\mathrm{e}^{\mathrm{i}(K_n x - \Omega_n t - \frac{\pi}{4})} \tag{4.4.66}$$

$$\delta_n = z + \mathrm{Re}\sum_0^N W_0 \frac{2^{5/2} c^3 t^{1/2}}{h\pi^{1/2}\omega_n^{7/2} x}[1-(x/ct)^2]^{3/4} \sin\left(\frac{\omega_n}{c}\frac{x/ct}{\sqrt{1-(x/ct)^2}}b\right)\sin\left(\frac{\omega_n}{\sqrt{1-(x/ct)^2}}\tau\right) \frac{\cos\mu_n(h-z)}{\sin\mu_n h} A_n\mu_n\mathrm{e}^{\mathrm{i}(K_n x - \Omega_n t - \frac{\pi}{4})} \tag{4.4.67}$$

Chapter 5

Gravity effects

In this chapter, the influence of gravity on the system initiates an exploration into the complex interaction between waves and particles within fluid systems. This derivation considers the dynamics governing Lagrangian particle motions and drift velocities in water waves.

It is important to note that in the study, the effect of gravity is not explicitly considered in the dispersion relation. However, in Equation 11 of [2], the effect of gravity is indeed incorporated into the dispersion relation. Abdolali and Kirby [2] focused primarily on the role of compressibility on tsunami propagation, and their analysis included the effect of gravity in the dispersion relation.

Beginning by solving the mechanics behind Lagrangian particle motions and Stokes drift velocities in water waves, laying the essential foundation. In the subsequent sections, the complex behaviours that shape fluid particle motion and drift velocities will be carried out, offering insights into their interactions in wave-induced phenomena.

The trajectories traced by particles as they navigate the dynamic forces at play are then proceeded to be uncovered, revealing their paths through fluid mediums. Additionally, Particle motion is investigated, and Taylor's expansion for drift velocity is applied, offering deeper insights into how particles respond to the forces exerted by waves.

while exploring the horizontal drift velocity and mean Stokes drift velocity, the complex relationship between horizontal and vertical fluid particle movements becomes evi-

dent. This understanding illuminates the complex ways in which particles move through the combined influences of gravitational and wave-induced forces.

This study concludes with the equation derivation for quantifying water transport by AGWs from submarine earthquakes. This practical application emphasizes how comprehension of fluid particle motions and drift velocities translates into a quantifiable impact assessment for complex wave systems generated by seismic events.

5.1 Impact of gravity on wave dynamics and fluid particle motion

Utilising the wave equation (3.1.1) and by applying the boundary conditions (4.1.2) and (4.1.3) and by employing a double Fourier transform where the poles influencing the contour integration originate from the dispersion relation present in the transformed potential. By reversing the transformation through contour integration, the velocity potential obtained by [51] is presented as follows:

$$\phi_0 = -\frac{W_0}{\pi} Re \int_{\omega_N}^{\infty} \mathrm{i}\, d\omega \sum_{1}^{N} A_n \frac{8\mu_n \sin(k_n b)\sin(\omega\tau)\cos(\mu_n z)}{\omega k_n^2 [2\mu_n h + \sin(2\mu_n h)]} \mathrm{e}^{ik_n|x| - \mathrm{i}\omega t} \tag{5.1.1}$$

To demonstrate the impact of gravitational forces, we start by presenting the pressure after the gravity taken into account from [49]:

$$P(x,y,z,t) = \sum_{n=1}^{N} \frac{\rho W_0}{\pi} \frac{8\mu_n \sin(K_n b)\sin(\Omega_n \tau)\cos(\mu_n z)}{K_n^2 [2\mu_n h + \sin(2\mu_n h)]} \left[\frac{2\pi}{\frac{x}{c} \frac{\omega_n^2}{(\Omega_n^2 - \omega_n^2)^{3/2}}} \right]^{1/2} \cos\left(K_n x - \Omega_n t - \frac{\pi}{4}\right) \tag{5.1.2}$$

we can analyze the ratio of the pressure before the gravity is taken into account (4.1.14) an after the gravity is taken into account (5.1.2) across the entire column section. Following some algebraic manipulation, we derive the following expression for this ratio:

$$\frac{\frac{2\cos(\mu-z)\sin(\mu(h-z))}{[2\mu h+\sin(2\mu h)]\mu h\sin(\mu h)}}{\frac{\mu h\cos(\mu z)}{2\mu h+\sin(2\mu h)}} \tag{5.1.3}$$

Subsequently, we aim to enhance comprehension by complementing the mathematical elucidation with a graphical representation. This graphical illustration (figure 5.1) is presented to provide a visual aid, thereby fostering a deeper understanding of the gravity effect.

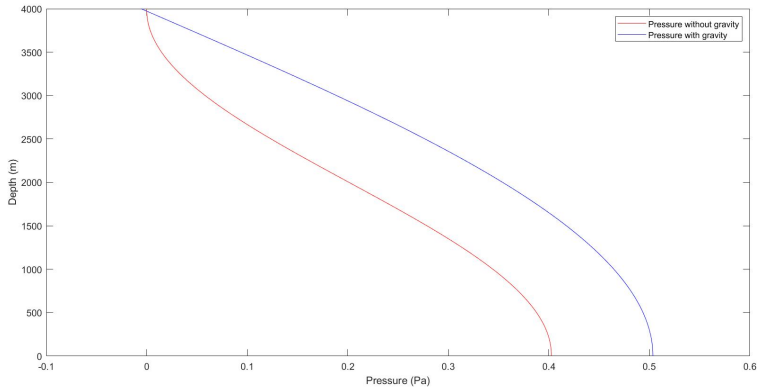

Figure 5.1: Pressure in the ocean: with and without gravity.

Figure 5.1 displays pressure profiles, contrasting scenarios with and without the influence of gravity. the first is pressure with gravity which showcases an increase from the surface towards the seabed, while the pressure with gravity exhibits non-zero values at the surface as it increases with depth. Notably, pressure values considering gravity are generally higher compared to those without gravitational effects, except near the surface.

Proceeding, by applying the stationary phase approximation to (5.1.1), the potential can be written as follows:

$$\phi_0 = \frac{-iW_0}{\pi} Re \sum_{n=1}^{N} A_n \frac{8\mu_n \sin(K_n b)\sin(\Omega_n \tau)\cos(\mu_n z)}{\Omega_n K_n^2 \left[2\mu_n h + \sin(2\mu_n h)\right]} \left[\frac{2\pi}{\frac{x}{c}\frac{\omega_n^2}{(\Omega_n^2-\omega_n^2)^{3/2}}}\right]^{1/2} e^{i(k_n|x|-\omega t-\frac{\pi}{4})} \tag{5.1.4}$$

The derivative of ϕ_0 with respect to x, y, and z after employing the stationary phase approximation yields expressions for the velocities in the horizontal and vertical directions as follows:

$$\phi_x = -\frac{iW_0}{\pi} Re \sum_{n=1}^{N} \frac{8\mu_n \sin(K_n b)\sin(\Omega_n \tau)\cos(\mu_n z)}{\Omega_n K_n^2 [2\mu_n h + \sin(2\mu_n h)]} \times \left[\frac{2\pi}{\frac{x}{c}\frac{\omega_n^2}{(\Omega_n^2-\omega_n^2)^{3/2}}}\right]^{1/2} e^{ik_n|x|-i\omega t-\frac{i\pi}{4}} (A_{n_x} + ik_n A_n) \tag{5.1.5}$$

$$\phi_y = -\frac{iW_0}{\pi} Re \sum_{n=1}^{N} \frac{8\mu_n \sin(K_n b)\sin(\Omega_n \tau)\cos(\mu_n z)}{\Omega_n K_n^2 [2\mu_n h + \sin(2\mu_n h)]} \times \left[\frac{2\pi}{\frac{x}{c}\frac{\omega_n^2}{(\Omega_n^2-\omega_n^2)^{3/2}}}\right]^{1/2} e^{ik_n|x|-i\omega t-\frac{i\pi}{4}} (A_{n_y}) \tag{5.1.6}$$

$$\phi_z = \frac{iW_0}{\pi} Re \sum_{n=1}^{N} A_n \frac{8\mu_n^2 \sin(K_n b)\sin(\Omega_n \tau)\sin(\mu_n z)}{\Omega_n K_n^2 [2\mu_n h + \sin(2\mu_n h)]} \times \left[\frac{2\pi}{\frac{x}{c}\frac{\omega_n^2}{(\Omega_n^2-\omega_n^2)^{3/2}}}\right]^{1/2} e^{ik_n|x|-i\omega t-\frac{i\pi}{4}} \tag{5.1.7}$$

These equations lead to the derivation of displacements:

$$\alpha_n = x_0 + \frac{\mathrm{i}W_0}{\pi} Re \sum_{n=1}^{N} \frac{8\mu_n \sin(K_n b)\sin(\Omega_n \tau)\cos(\mu_n z)}{\Omega_n K_n^2 [2\mu_n h + \sin(2\mu_n h)]} \times \left[\frac{2\pi}{\frac{x}{c}\frac{\omega_n^2}{(\Omega_n^2 - \omega_n^2)^{3/2}}} \right]^{1/2} \mathrm{e}^{ik_n|x| - \mathrm{i}\omega t - \frac{\mathrm{i}\pi}{4}} (A_{n_x} + ik_n A_n) \tag{5.1.8}$$

$$\beta_n = y + \frac{\mathrm{i}W_0}{\pi} Re \sum_{n=1}^{N} \frac{8\mu_n \sin(K_n b)\sin(\Omega_n \tau)\cos(\mu_n z)}{\Omega_n K_n^2 [2\mu_n h + \sin(2\mu_n h)]} \times \left[\frac{2\pi}{\frac{x}{c}\frac{\omega_n^2}{(\Omega_n^2 - \omega_n^2)^{3/2}}} \right]^{1/2} \mathrm{e}^{ik_n|x| - \mathrm{i}\omega t - \frac{\mathrm{i}\pi}{4}} (A_{n_y}) \tag{5.1.9}$$

$$\delta_n = z - \frac{\mathrm{i}W_0}{\pi} Re \sum_{n=1}^{N} A_n \frac{8\mu_n^2 \sin(K_n b)\sin(\Omega_n \tau)\sin(\mu_n z)}{\Omega_n K_n^2 [2\mu_n h + \sin(2\mu_n h)]} \times \left[\frac{2\pi}{\frac{x}{c}\frac{\omega_n^2}{(\Omega_n^2 - \omega_n^2)^{3/2}}} \right]^{1/2} \mathrm{e}^{ik_n|x| - \mathrm{i}\omega t - \frac{\mathrm{i}\pi}{4}} \tag{5.1.10}$$

The movement of particles is demonstrated in Figure (3.4), showing how Stokes drift velocities for gravity waves and AGWs dynamically shape water particles' behaviour across various depths.

In ocean dynamics, this exploration delves into the hidden field of deep orbital velocities, revealing the appropriate interplay of wave parameters and fluid particle trajectories. From the oscillations of water particles to the influence of AGWs, Below the surface of the ocean lies a captivating realm of constant motion that shapes the currents in its deep waters.

5.2 Lagrangian fluid particle motions and Stokes drift velocities in water waves

This section starts with the fundamental concepts related to the velocity potential and the Lagrangian position, followed by the derivation of the horizontal (U), (V), and vertical (W) components of the Stokes drift velocity. This analysis involves various derivatives and expansions to approximate the mean Lagrangian velocities. Beginning by recalling the expression for the velocity potential ϕ_0, which is given by:

$$\phi_0 = -\frac{W_0}{\pi} Re \int_{\omega_N}^{\infty} \mathrm{i}\, d\omega \sum_{1}^{N} A_n \frac{8\mu_n \sin(k_n b)\sin(\omega\tau)\cos(\mu_n z)}{\omega k_n^2 [2\mu_n h + \sin(2\mu_n h)]} \mathrm{e}^{ik_n|x| - \mathrm{i}\omega t} \tag{5.2.11}$$

where the summation is carried out for discrete wave components indexed by n. The integral over ω accounts for the temporal frequency.

Equation (5.2.11) can be simplified to:

This equation represents the velocity potential in terms of A_n, and trigonometric functions.

Now, let's consider the partial derivatives of the velocity potential with respect to x, y, and z. The derivatives are given by:

$$\phi_x = Re\left\{-\frac{\mathrm{i}W_0}{\pi} \int_{\omega_N}^{\infty} d\omega \sum_{1}^{N} \frac{8\mu_n \sin(k_n b)\sin(\omega\tau)}{\omega k_n^2 [2\mu_n h + \sin(2\mu_n h)]} \cos(\mu_n z)[A_x \mathrm{e}^{ik_n|x| - \mathrm{i}\omega t} + \mathrm{i}kA\mathrm{e}^{ik_n|x| - \mathrm{i}\omega t}]\right\} \tag{5.2.12}$$

$$\phi_y = Re\left\{-\frac{\mathrm{i}W_0}{\pi} \int_{\omega_N}^{\infty} d\omega \sum_{1}^{N} \frac{8\mu_n \sin(k_n b)\sin(\omega\tau)}{\omega k_n^2 [2\mu_n h + \sin(2\mu_n h)]} A_y \cos(\mu_n z)\mathrm{e}^{ik_n|x| - \mathrm{i}\omega t}\right\} \tag{5.2.13}$$

$$\phi_z = -Re\left\{-\frac{\mathrm{i}W_0}{\pi}\int_{\omega_N}^{\infty} d\omega \sum_{1}^{N} \frac{8\mu_n \sin(k_n b)\sin(\omega\tau)}{\omega k_n^2[2\mu_n h + \sin(2\mu_n h)]}\mu A \sin(\mu_n z)\mathrm{e}^{ik_n|x|-\mathrm{i}\omega t}\right\} \quad (5.2.14)$$

These equations describe the spatial variations of the velocity potential in the horizontal (ϕ_x and ϕ_y) and vertical (ϕ_z) directions.

Moving forward, by integrating the above expressions with respect to t, obtaining:

$$\int \phi_x dt = Re\frac{-\frac{\mathrm{i}W_0}{\pi}\int_{\omega_N}^{\infty} d\omega \sum_{1}^{N} \frac{8\mu_n \sin(k_n b)\sin(\omega\tau)}{\omega k_n^2[2\mu_n h+\sin(2\mu_n h)]}\cos(\mu z)}{-\mathrm{i}\omega}[A_x\mathrm{e}^{ik_n|x|-\mathrm{i}\omega t} + \mathrm{i}Ak\mathrm{e}^{ik_n|x|-\mathrm{i}\omega t}] \quad (5.2.15)$$

$$\int \phi_y dt = Re\frac{-\frac{\mathrm{i}W_0}{\pi}\int_{\omega_N}^{\infty} d\omega \sum_{1}^{N} \frac{8\mu_n \sin(k_n b)\sin(\omega\tau)}{\omega k_n^2[2\mu_n h+\sin(2\mu_n h)]}A_y\cos(\mu z)}{-\mathrm{i}\omega}\mathrm{e}^{ik_n|x|-\mathrm{i}\omega t} \quad (5.2.16)$$

$$\int \phi_z dt = -Re\frac{-\frac{\mathrm{i}W_0}{\pi}\int_{\omega_N}^{\infty} d\omega \sum_{1}^{N} \frac{8\mu_n \sin(k_n b)\sin(\omega\tau)}{\omega k_n^2[2\mu_n h+\sin(2\mu_n h)]}\mu A\sin(\mu z)}{-\mathrm{i}\omega}\mathrm{e}^{ik_n|x|-\mathrm{i}\omega t} \quad (5.2.17)$$

Next, let's delve into the Lagrangian position components ξ_x, ξ_y, and ξ_z. These components represent the horizontal and vertical positions of Lagrangian particles.

For ξ_x :

$$\xi_x = x + Re\int \phi_x dt = x + Re\frac{-\frac{\mathrm{i}W_0}{\pi}\int_{\omega_N}^{\infty} d\omega \sum_{1}^{N} \frac{8\mu_n \sin(k_n b)\sin(\omega\tau)}{\omega k_n^2[2\mu_n h+\sin(2\mu_n h)]}\cos(\mu z)}{-\mathrm{i}\omega}[A_x\mathrm{e}^{ik_n|x|-\mathrm{i}\omega t} + \mathrm{i}Ak\mathrm{e}^{ik_n|x|-\mathrm{i}\omega t}] \quad (5.2.18)$$

This equation relates the Lagrangian position in the x direction to the spatial and temporal variations of the velocity potential.

Similarly, for ξ_y:

$$\xi_y = y + Re\int \phi_y dt = y + Re\frac{-\frac{iW_0}{\pi}\int_{\omega_N}^{\infty} d\omega \sum_1^N \frac{8\mu_n \sin(k_n b)\sin(\omega\tau)}{\omega k_n^2[2\mu_n h + \sin(2\mu_n h)]} A_y \cos(\mu z)}{-i\omega} e^{ik_n|x| - i\omega t} \tag{5.2.19}$$

And for ξ_z:

$$\xi_z = z + Re\int \phi_z dt = z - Re\frac{-\frac{iW_0}{\pi}\int_{\omega_N}^{\infty} d\omega \sum_1^N \frac{8\mu_n \sin(k_n b)\sin(\omega\tau)}{\omega k_n^2[2\mu_n h + \sin(2\mu_n h)]} \mu A \sin(\mu z)}{-i\omega} e^{ik_n|x| - i\omega t} \tag{5.2.20}$$

These equations establish the Lagrangian position components as functions of spatial and temporal terms.

In order to estimate the mean Lagrangian velocities U, V, and W, the application of Taylor expansions and differentiation is needed. Starting with the horizontal component U, obtaining:

$$\begin{aligned} U &= (\xi_x - x)\frac{\partial^2 \xi_x}{\partial x \partial t} + (\xi_y - y)\frac{\partial^2 \xi_x}{\partial y \partial t} + (\xi_z - z)\frac{\partial^2 \xi_x}{\partial z \partial t} \\ &= Re\left\{ \frac{-\frac{iW_0}{\pi}\int_{\omega_N}^{\infty} d\omega \sum_1^N \frac{8\mu_n \sin(k_n b)\sin(\omega\tau)}{\omega k_n^2[2\mu_n h + \sin(2\mu_n h)]}^2 \cos^2(\mu z)}{-i\omega} e^{2(ik_n|x| - i\omega t)} \right. \\ &\times \left[A_x A_{xx} - 3AA_x k^2 + A_y A_{xy} - iA^2 k^3 + iAA_{xx} k + 2iA_x^2 k + iA_y^2 k\right] \\ &\left. + \frac{-\frac{iW_0}{\pi}\int_{\omega_N}^{\infty} d\omega \sum_1^N \frac{8\mu_n \sin(k_n b)\sin(\omega\tau)}{\omega k_n^2[2\mu_n h + \sin(2\mu_n h)]}^2 \mu^2 \sin^2(\mu z)}{-i\omega} e^{2(ik_n|x| - i\omega t)} \left[AA_x + A^2 k\right] \right\} \end{aligned} \tag{5.2.21}$$

Similarly, for V:

$$
\begin{aligned}
V &= (\xi_x - x)\frac{\partial^2 \xi_y}{\partial x \partial t} + (\xi_y - y)\frac{\partial^2 \xi_y}{\partial y \partial t} + (\xi_z - z)\frac{\partial^2 \xi_y}{\partial z \partial t} \\
&= Re\left\{ \frac{\frac{iW_0}{\pi}\int_{\omega_N}^{\infty} d\omega \sum_1^N \frac{8\mu_n \sin(k_n b)\sin(\omega\tau)}{\omega k_n^2[2\mu_n h + \sin(2\mu_n h)]}^2 \cos^2(\mu z)}{i\omega} e^{2(ik_n|x| - i\omega t)} \right. \\
&\times \left[A_x A_{yx} - AA_y k^2 + A_y A_{yy} - AA_{yx} k + A_x A_y k\right] \\
&\left. + \frac{\frac{iW_0}{\pi}\int_{\omega_N}^{\infty} d\omega \sum_1^N \frac{8\mu_n \sin(k_n b)\sin(\omega\tau)}{\omega k_n^2[2\mu_n h + \sin(2\mu_n h)]}^2 \mu^2 \sin^2(\mu z)}{i\omega} AA_y e^{2(ik_n|x| - i\omega t)} \right\}
\end{aligned}
\tag{5.2.22}
$$

And finally, for the vertical component W:

$$
\begin{aligned}
W &= (\xi_x - x)\frac{\partial^2 \xi_z}{\partial x \partial t} + (\xi_y - y)\frac{\partial^2 \xi_z}{\partial y \partial t} + (\xi_z - z)\frac{\partial^2 \xi_z}{\partial z \partial t} \\
&= Re\left\{ \frac{-\frac{iW_0}{\pi}\int_{\omega_N}^{\infty} d\omega \sum_1^N \frac{8\mu_n \sin(k_n b)\sin(\omega\tau)}{\omega k_n^2[2\mu_n h + \sin(2\mu_n h)]}^2 \mu}{i\omega} \cos(\mu z)\sin(\mu z) e^{2(ik_n|x| - i\omega t)} \right. \\
&\times \left[A_x^2 + A_y^2 + 2ikAA_x - k^2 A^2\right] \\
&\left. + \frac{-\mu^3 - \frac{iW_0}{\pi}\int_{\omega_N}^{\infty} d\omega \sum_1^N \frac{8\mu_n \sin(k_n b)\sin(\omega\tau)}{\omega k_n^2[2\mu_n h + \sin(2\mu_n h)]}^2}{i\omega} \sin(\mu z)\cos(\mu z) A^2 e^{2(ik_n|x| - i\omega t)} \right\}
\end{aligned}
\tag{5.2.23}
$$

Finally, the leading modes U_0 and V_0 are as follows:

$$
U_0 = Re\frac{-\frac{iW_0}{\pi}\int_{\omega_N}^{\infty} d\omega \sum_1^N \frac{8\mu_n \sin(k_n b)\sin(\omega\tau)}{\omega k_n^2[2\mu_n h + \sin(2\mu_n h)]}^2 k}{\omega} e^{2(ik_n|x| - i\omega t)} \left[A^2 k^2 \cos^2(\mu_n z) + A_y^2 \cos^2(\mu_n z) + A^2 \mu_n^2 \sin^2(\mu_
\tag{5.2.24}
$$

$$
V_0 = Re\frac{-\frac{iW_0}{\pi}\int_{\omega_N}^{\infty} d\omega \sum_1^N \frac{8\mu_n \sin(k_n b)\sin(\omega\tau)}{\omega k_n^2[2\mu_n h + \sin(2\mu_n h)]}^2 AA_y}{\omega} e^{2(ik_n|x| - i\omega t)} \left[\mu_n^2 \sin^2(\mu_n z) - k^2 \cos^2(\mu_n z)\right]
\tag{5.2.25}
$$

In summary, This exploration has led to derive fundamental expressions for the Lagrangian positions ξ_x, ξ_y, and ξ_z, unveiling the spatial coordinates that describe the trajectories of particles in water wave systems. Additionally, the mean Lagrangian velocities U, V, and W associated with these positions have been derived. These calculations have required complicated differentiation, integrations, and Taylor expansions, illuminating the complex interaction between the defining wave parameters and the complex motions of individual particles. This analysis contributes to a deeper understanding of the dynamic interactions between waves and particles, underscoring the significance of unravelling the complexities that underlie wave-induced perturbations.

5.3 Dynamics of Lagrangian fluid particle motion and drift velocities in water waves

In this section, a study of fluid particle behaviour and associated drift velocities within water wave systems is conducted. This investigation begins by introducing a fundamental equation defining the potential ϕ, which intricately combines wave parameters and fluid particle coordinates. This equation forms the base of this study, enabling an in-depth exploration of Lagrangian positions and velocities.

Through some differentiation and expansion, expressions for the horizontal and vertical components of Lagrangian positions and velocities are derived. This mathematical framework allows to quantitatively analyze the relationships between fluid particle coordinates, wave parameters, and time. Moreover, it provides insights into how particles respond to wave-induced forces and contribute to water flow patterns. This analysis uncovers the dynamics that highlight fluid particle motion in the complex interaction of water waves. Starting with the velocity potential:

$$\phi = \frac{-H_n \omega \cos(\mu_n z)}{2\mu_n \sin(\mu_n h)} A_n \sin(k_n x - \omega t) \tag{5.3.26}$$

which forms the basis for the subsequent analysis of Lagrangian positions and velocities

in water wave systems. For brevity, let

$$B = \frac{-\eta\omega}{\mu_n \sin(\mu_n h)}, \quad \eta = \frac{H_n}{2} \quad \text{and} \quad \theta = k_n x - \omega t \tag{5.3.27}$$

Here, B describes the wave's influence on fluid particle motion, while θ relates to the fluid particle's position in space and time. This simplifies the potential equation to:

$$\phi = BA_n \cos(\mu_n z) \sin\theta \tag{5.3.28}$$

The partial derivative of ϕ with respect to x, y, and z are respectively given by:

$$\phi_X = B\cos(\mu_n z)[\epsilon^2 A_{nx} \sin\theta + A_n k \cos\theta] \tag{5.3.29}$$

$$\phi_Y = B\cos(\mu_n z)\epsilon A_{ny} \sin\theta \tag{5.3.30}$$

$$\phi_z = -B\mu_n \sin(\mu_n z) A_n \sin\theta \tag{5.3.31}$$

Equations (5.3.29), (5.3.30), and (5.3.31) provide the partial derivatives of ϕ with respect to the spatial coordinates x, y, and z, respectively. These derivatives are crucial for analyzing the Lagrangian positions and velocities in the wave system.

Integrating with respect to t, obtaining:

$$\int \phi_X dt = B\cos(\mu_n z)\left[\frac{\epsilon^2 A_x}{\omega}\cos\theta - \frac{A_n k_n}{\omega}\sin\theta\right] \tag{5.3.32}$$

$$\int \phi_Y dt = \frac{B}{\omega}\cos(\mu_n z)\epsilon A_y \cos\theta \tag{5.3.33}$$

$$\int \phi_z dt = -\frac{B}{\omega}\mu_n \sin(\mu_n z) A_n \cos\theta \tag{5.3.34}$$

These equations represent the time integration of the derivatives, providing insight

into the cumulative effect of potential variations on the Lagrangian positions over time.

Now, let's consider the horizontal and vertical components, ξ_x, ξ_y, and ξ_z, of the Lagrangian position ξ:

$$\begin{aligned}\xi_x &= x + \int \phi_X dt \\ &= x + B\cos(\mu_n z)\left[\frac{\epsilon^2 A_x}{\omega}\cos\theta - \frac{A_n k_n}{\omega}\sin\theta\right]\end{aligned} \tag{5.3.35}$$

$$\begin{aligned}\xi_y &= y + \int \phi_Y dt \\ &= y + \frac{B}{\omega}\cos(\mu_n z)\epsilon A_y \cos\theta\end{aligned} \tag{5.3.36}$$

$$\begin{aligned}\xi_z &= z + \int \phi_z dt \\ &= z - \frac{B}{\omega}\mu_n \sin(\mu_n z) A_n \cos\theta\end{aligned} \tag{5.3.37}$$

Equations (5.3.35), (5.3.36), and (5.3.37) define the Lagrangian positions ξ_x, ξ_y, and ξ_z by integrating the corresponding derivatives over time. These expressions describe how particles are displaced within the wave system.

Establishing a Taylor expansion of the horizontal component x, by differentiating Equation (5.3.35) with respect to x, y, and z, and then with respect to t. This yields:

$$\frac{\partial^2 \xi_x}{\partial X \partial t} = B\cos(\mu_n z)\left[2\epsilon^2 A_x k_n \cos\theta + \epsilon^4 A_{xx}\sin\theta - A_n k_n^2 \sin\theta\right] \tag{5.3.38}$$

$$\frac{\partial^2 \xi_x}{\partial Y \partial t} = B\cos(\mu_n z)[\epsilon^3 A_{xy}\sin\theta + \epsilon A_y k_n \cos\theta] \tag{5.3.39}$$

$$\frac{\partial^2 \xi_x}{\partial z \partial t} = -B\mu_n \sin(\mu_n z)[\epsilon^2 A_x \sin\theta + A_n k_n \cos\theta] \tag{5.3.40}$$

Equations (5.3.38), (5.3.39), and (5.3.40) provide the second-order partial derivatives of ξ_x with respect to the spatial coordinates x, y, and z and t. These derivatives

describe the acceleration and are crucial for estimating the horizontal component of the Stokes drift velocity.

The horizontal component U of the Stokes drift velocity is estimated by using a Taylor expansion of Equation (5.3.29) about ξ_x. After some algebraic manipulations, yielding the expression:

$$\begin{aligned} U &= (\xi_x - x)\frac{\partial^2 \xi_x}{\partial x \partial t} + (\xi_y - y)\frac{\partial^2 \xi_x}{\partial y \partial t} + (\xi_z - z)\frac{\partial^2 \xi_x}{\partial z \partial t} \\ &= \frac{B^2}{\omega}\cos^2(\mu_n z)[(2\epsilon^4 A_x^2 k_n + \epsilon^2 A_y^2 k_n)\cos^2\theta - (\epsilon^4 A_n A_{xx} k_n - A_n^2 k_n^3)\sin^2\theta \\ &+ (\epsilon^6 A_x A_{xx} + \epsilon^4 A_y A_{xy} - 3\epsilon^2 A_n A_x k_n^2)\sin\theta\cos\theta] \\ &+ \frac{B^2\mu_n^2}{\omega}\sin^2(\mu_n z)[\epsilon^2 A_n A_x \cos\theta\sin\theta + A_n^2 k_n \cos^2\theta] \end{aligned} \tag{5.3.41}$$

Equation (5.3.41) represents the horizontal drift component U of the Stokes drift velocity. It accounts for the intricate interplay between wave parameters, Lagrangian positions, and time derivatives.

Hence, the leading mode U_0, which uncovers intricate fluid particle dynamics within wave-induced perturbations, can be obtained.

$$\begin{aligned} U_0 &= \frac{B^2}{\omega}\cos^2(\mu_n z)A_n^2 k_n^3 \sin^2\theta + \frac{B^2\mu_n^2}{\omega}\sin^2(\mu_n z)A_n^2 k_n \cos^2\theta \\ &= \frac{B^2 A_n^2 k_n}{\omega}(k_n^2 \cos^2(\mu_n z)\sin^2\theta + \mu_n^2 \sin^2(\mu_n z)\cos^2\theta) \end{aligned} \tag{5.3.42}$$

Now, let's investigate the horizontal component of the drift velocity V. By differentiating Equation (5.3.36) with respect to x, y, and z, and then with respect to t, obtaining:

$$\frac{\partial^2 \xi_y}{\partial x \partial t} = B\cos(\mu_n z)[\epsilon^3 A_{yx}\sin\theta + \epsilon A_y k_n \cos\theta] \tag{5.3.43}$$

$$\frac{\partial^2 \xi_y}{\partial y \partial t} = B\ cos(\mu_n z)\epsilon^2 A_{yy}\sin\theta \tag{5.3.44}$$

$$\frac{\partial^2 \xi_y}{\partial z \partial t} = -B\mu_n \sin(\mu_n z)\epsilon A_y \sin\theta \tag{5.3.45}$$

These equations describe the second-order partial derivatives of ξ_y with respect to x, y, z, and t. These derivatives play a key role in estimating the vertical component of the Stokes drift velocity.

Then V is estimated by using a Taylor expansion of (5.3.30) about ξ_y to estimate the mean Lagrangian velocity with some algebra to get

$$\begin{aligned} V &= (\xi_x - x)\frac{\partial^2 \xi_y}{\partial x \partial t} + (\xi_y - y)\frac{\partial^2 \xi_y}{\partial y \partial t} + (\xi_z - z)\frac{\partial^2 \xi_y}{\partial z \partial t} \\ &= \frac{B^2}{\omega}\cos^2(\mu_n z)[\epsilon^3 A_x A_y K_n \cos^2\theta - \epsilon^3 A_n A_{yx} k_n \sin^2\theta \\ &+ (\epsilon^5 A_x A_{yx} - \epsilon A_n A_y k_n^2 + \epsilon^3 A_y A_{yy})\sin\theta\cos\theta] \\ &+ \frac{B^2\mu^2}{\omega} A A_y \sin^2(\mu z)\epsilon A_n A_y \sin\theta\cos\theta \end{aligned} \tag{5.3.46}$$

Now, for the vertical component W, (5.3.37) is differentiated with respect to x, y, and z, and then integrated with respect to t to obtain

$$\frac{\partial^2 \xi_z}{\partial x \partial t} = -B\mu_n \sin(\mu_n z)[\epsilon^2 A_x \sin\theta + A_n k_n \cos\theta] \tag{5.3.47}$$

$$\frac{\partial^2 \xi_z}{\partial y \partial t} = -B\mu_n \sin(\mu_n z)\epsilon A_y \sin\theta \tag{5.3.48}$$

and

$$\frac{\partial^2 \xi_z}{\partial z \partial t} = -B\mu_n^2 \cos(\mu_n z) A_n \sin\theta \tag{5.3.49}$$

The vertical component W of the Stokes drift velocity is estimated by using a Taylor expansion of Equation (5.3.31) about ξ_z. After algebraic manipulation, to find:

$$
\begin{aligned}
W &= (\xi_x - x)\frac{\partial^2 \xi_z}{\partial x \partial t} + (\xi_y - y)\frac{\partial^2 \xi_z}{\partial y \partial t} + (\xi_z - z)\frac{\partial^2\ xi_z}{\partial z \partial t} \\
&= \frac{B^2 \mu_n}{\omega} \sin(\mu_n z)\cos(\mu_n z)[\epsilon^2 A_n A_x k_n \sin^2\theta - \epsilon A_n A_x k_n \cos^2\theta \\
&+ (\mu_n^2 A_n^2 - \epsilon^4 A_x^2 + A_n^2 k_n^2 - \epsilon^2 A_y^2)\sin\theta\cos\theta]
\end{aligned}
\tag{5.3.50}
$$

Equation (5.3.50) describes the vertical drift component W of the Stokes drift velocity. It showcases the intricate interplay between wave parameters, Lagrangian positions, and time derivatives.

The averaging of the quantities U and V over time:

$$
\overline{U} = \frac{1}{T}\int_0^T u(t)\,dt \tag{5.3.51}
$$

$$
\overline{V} = \frac{1}{T}\int_0^T v(t)\,dt \tag{5.3.52}
$$

yields the following expressions:

$$
\begin{aligned}
\overline{U} &= \frac{B^2}{\omega}\cos^2(\mu_n z)[\epsilon^4 A_x^2 k_n + \frac{1}{2}\epsilon^2 A_y^2 k_n - \frac{1}{2}\epsilon^4 A_n A_{xx} k_n + \frac{1}{2}A_n^2 k_n^3) \\
&+ \frac{B^2 \mu_n^2}{2\omega}\sin^2(\mu_n z) A_n^2 k_n
\end{aligned}
\tag{5.3.53}
$$

This equation represents the mean horizontal Stokes drift velocity ($\overline{U}$) after averaging over time. It accounts for the complex interplay of wave parameters and fluid particle dynamics, shedding light on the horizontal motion of particles within the wave-induced perturbations.

The leading mode:

$$
\overline{U}_0 = \frac{\eta^2}{2}\frac{A^2 \omega k_n}{\sin^2(\mu_n h)}\left[\frac{k_n^2}{\mu_n^2}\cos^2(\mu_n z) + \sin^2(\mu_n z)\right] \tag{5.3.54}
$$

Here, $\overline{U}_0$ characterizes the dominant horizontal drift mode within the wave system. This mode showcases the influence of wave parameters, water depth, and fluid particle behaviour on the averaged horizontal motion.

Similarly, the averaged vertical drift velocity ($\overline{V}$) is given by:

$$\overline{V} = \frac{B^2}{\omega}\cos^2(\mu_n z)\left[\frac{\epsilon^2}{2}A_x A_y k_n - \frac{\epsilon^2}{2}A_n A_{yx} k_n\right] \tag{5.3.55}$$

This equation describes the mean vertical motion of particles within wave-induced perturbations. The relationship between wave parameters, fluid particle dynamics, and vertical motion is unveiled through the expression for $\overline{V}$.

The leading mode for vertical drift is:

$$\overline{V}_0 = \frac{\eta^2}{2}\frac{k_n\omega}{\mu_n^2\sin^2(\mu_n h)}\cos^2(\mu_n z)\left[A_x A_y - A A_{yx}\right] \tag{5.3.56}$$

This mode captures the dominant vertical drift behaviour and illustrates the interplay between wave characteristics, water depth, and fluid particle movements in the vertical direction. Where $\eta(x,y,t)$ the wave height is defined by [50] :

$$\eta(x,y,t) = \sum_{n=1}^{N}\frac{W_0}{g\pi}\frac{8\mu_n\sin(K_n b)\sin(\Omega_n\tau)\cos(\mu_n h)}{K_n^2[2\mu_n h + \sin(2\mu_n h)]}\left[\frac{2\pi}{\frac{x}{c}\frac{\omega_n^2}{(\Omega_n^2-\omega_n^2)^{3/2}}}\right]^{1/2} \tag{5.3.57}$$

The wave number K_n and frequency Ω_n are given by:

$$K_n = \frac{\omega_n x}{c^2 t\sqrt{1-(\frac{x}{ct})^2}} \tag{5.3.58}$$

$$\Omega_n = \frac{\omega_n}{\sqrt{1-(\frac{x}{ct})^2}} \tag{5.3.59}$$

These expressions define the wave number and frequency associated with each mode,

taking into account the spatial and temporal dimensions.

The amplitude function (4.1.15) characterizes the behaviour of each mode and involves the complex interplay between trigonometric and exponential terms, further contributing to the description of fluid particle dynamics within the wave system.

In the study, the critical time (t) is used to signify the moment when the AGWs generated by the fault rupture pass the edges of the fault area [31], where:

$$t = \frac{\sqrt{(y^2) + (x^2)}}{c}. \tag{5.3.60}$$

5.4 Derivation of the drift velocity by AGWs from submarine earthquake

The following section introduces the fundamental concepts and equations related to the two-dimensional compressible velocity potential proposed by [22]. This potential plays a crucial role in unravelling the intricate fluid particle dynamics within wave-induced perturbations. Starting by recalling the compressible velocity potential [22]:

$$\phi_n = -\frac{H_n}{2}\frac{\omega}{\lambda_n}\frac{\cosh[\lambda_n(h+z)]}{\sinh(\lambda_n h)}\sin(k_n x - \omega t) \tag{5.4.61}$$

where the hyperbolic functions cosh and sinh relate to the wave-induced perturbations. Additionally, let the amplitude of the wave $\eta = \frac{H_n}{2}$ and $\lambda_n = \mathrm{i}\mu_n$. substituting into (5.4.61), a more simplified form emerges:

$$\phi_n = -\frac{\eta\omega}{\mathrm{i}\mu}\frac{\cos(\mu_n z)}{\mathrm{i}\sin(\mu_n h)}\sin(k_n x - \omega t) \tag{5.4.62}$$

Further simplification leads to:

$$\phi_n = \frac{\eta\omega}{\mu}\frac{\cos(\mu_n z)}{\sin(\mu_n h)}\sin\theta \tag{5.4.63}$$

where $\theta = kx - \omega t$. Deriving the partial derivatives of ϕ with respect to x and z is important for the subsequent analyses. Starting by the derivative ϕ_x which is given by:

$$\frac{\partial\phi_n}{\partial x} = \frac{\eta\omega k\cos(\mu_n z)}{\mu_n \sin(\mu_n h)}\cos\theta \tag{5.4.64}$$

This equation illustrates the role of wave parameters and the spatial distribution in the horizontal direction. Similarly, the derivative ϕ_z is expressed as:

$$\frac{\partial\phi_n}{\partial z} = -\frac{\eta\omega\sin(\mu_n z)}{\sin(\mu_n h)}\sin\theta \tag{5.4.65}$$

This equation offers insights into the vertical dynamics influenced by wave-induced perturbations.

Integrating these derivatives over time provides valuable information. The integration of ϕ_x with respect to time (t) yields:

$$\int \phi_x dt = -\frac{\eta k\cos(\mu_n z)}{\mu_n \sin(\mu_n h)}\sin\theta \tag{5.4.66}$$

Likewise, the integration of ϕ_z with respect to t results in:

$$\int \phi_z dt = -\frac{\eta\sin(\mu_n z)}{\sin(\mu_n h)}\cos\theta \tag{5.4.67}$$

These integrations elucidate the time-averaged behaviors of the potential and its derivatives.

The horizontal and vertical components, ξ_x and ξ_z, of the Lagrangian position are defined as follows:

$$\xi_x = x + \int \phi_x dt = x - \frac{\eta k \cos(\mu_n z)}{\mu_n \sin(\mu_n h)} \sin\theta \tag{5.4.68}$$

and

$$\xi_z = z + \int \phi_z dt = z - \frac{\eta \sin(\mu_n z)}{\sin(\mu_n h)} \cos\theta \tag{5.4.69}$$

These equations provide insights into the Lagrangian position changes influenced by wave-induced perturbations and their interaction with time.

A key outcome of this analysis is the estimation of the horizontal component U of the Stokes drift velocity. This estimation is facilitated by using a Taylor expansion of (5.4.64) around ξ_x to estimate the mean Lagrangian velocity U:

$$\begin{aligned} U &= (\xi_x - x)\left(\frac{\partial^2 \xi}{\partial x \partial t}\right) + (\xi_z - z)\left(\frac{\partial^2 \xi}{\partial z \partial t}\right) \\ &= \left[-\frac{\eta k \cos(\mu_n z)}{\mu_n \sin(\mu_n h)} \sin\theta\right] \cdot \left[-\frac{\eta \omega k^2 \cos(\mu_n z)}{\mu_n \sin(\mu_n h)} \sin\theta\right] \\ &\quad + \left[-\frac{\eta \sin(\mu_n z)}{\sin(\mu_n h)} \cos\theta\right] \cdot \left[-\frac{\eta \omega \sin(\mu_n z)}{\sin(\mu_n h)} \cos\theta\right] \\ &= \frac{\eta^2 k \omega}{\sin^2(\mu_n h)} \left[\frac{k^2}{\mu_n^2} \cos^2(\mu_n z) \sin^2\theta + \sin^2(\mu_n z) \cos^2\theta\right] \end{aligned} \tag{5.4.70}$$

To understand the mean drift velocity more comprehensively, time averaging is applied to the equation over time, resulting in:

$$\overline{U} = \frac{1}{t} \int_0^t \frac{\eta^2 k_n \omega}{\sin^2(\mu_n h)} \left(\frac{k_n^2}{\mu^2} \cos^2(\mu_n z) + \sin^2(\mu_n z) \cos^2\theta\right) dt \tag{5.4.71}$$

Further simplification leads to the expression:

$$U = \frac{\eta^2 k_n \omega}{2\sin^2(\mu_n h)} \left(\frac{k_n^2}{\mu^2} \cos^2(\mu_n z) + \sin^2(\mu_n z) \right) \tag{5.4.72}$$

The mean drift velocity is obtained by averaging over depth, wavelength $L = \frac{2\pi}{k}$, and period $T = \frac{2\pi}{\omega}$, yielding:

$$\begin{aligned} D_n &= \frac{1}{hLT} \int_0^h \int_x^{x+L} \int_0^T \frac{\eta^2 k_n \omega}{2\sin^2(\mu_n h)} \left(\frac{k_n^2}{\mu^2} \cos^2(\mu_n z) + \sin^2(\mu_n z) \right) dt dx dz \\ &= \frac{\eta^2 k_n \omega}{4\sin^2(\mu_n h)} \left[\frac{k_n^2}{\mu_n^2} \left(1 + \frac{\sin(2\mu h)}{2\mu} \right) + \left(1 - \frac{\sin(2\mu h)}{2\mu} \right) \right] \end{aligned} \tag{5.4.73}$$

This equation encapsulates the mean drift velocity and its dependence on wave parameters and depth. The integrals and their outcomes underscore the intricate dynamics of particles within the context of wave-induced perturbations. The concepts presented in this section lay the foundation for understanding and analyzing fluid particle behaviour in the presence of wave-induced perturbations. The equations derived here form the basis for further investigations and explorations in this field. The equations consider the interaction of wave parameters, depth, and time to determine the mean drift velocity experienced by particles in the water.
It's noteworthy that the integrals in the expression involve trigonometric functions, namely $\sin^2 x$ and $\cos^2 x$, are:

$$\begin{aligned} \int \sin^2 x dx &= \frac{1}{2}x - \frac{1}{4}\sin(2x) \\ \int \cos^2 x dx &= \frac{1}{2}x + \frac{1}{4}\sin(2x) \end{aligned} \tag{5.4.74}$$

These trigonometric integrals play a fundamental role in evaluating the resulting expression for D_n.

While (5.4.73) introduce the concept of integrating D_n over the whole depth, the expression for D_n when integrated over the section of h is as follows:

$$
\begin{aligned}
D_n &= \frac{1}{z_2 - z_1} \int_{z_1}^{z_2} \frac{\eta^2 k_n \omega}{2\sin^2(\mu_n h)} \left(\frac{k_n^2}{\mu_n^2} \cos^2(\mu_n z) + \sin^2(\mu_n z) \right) dz \\
&= \frac{\eta^2 k_n \omega}{4(z_2 - z_1)\sin^2(\mu_n h)} \left[\frac{k_n^2}{\mu_n^2} \left(\frac{\sin(2\mu_n z_2) + 2\mu_n z_2 - \sin(2\mu_n z_1) - 2\mu_n z_1}{2\mu_n} \right) \right. \\
&\quad \left. + \frac{\sin(2\mu_n z_1) - 2\mu_n z_1 - \sin(2\mu_n z_2) + 2\mu_n z_2}{2\mu_n} \right]
\end{aligned} \tag{5.4.75}
$$

The terms within the equation reveal the interdependence of various factors. The depth range of integration, from z_1 to z_2, illustrates the consideration of vertical stratification in the ocean. This paves the way for the formulation of a fundamental metric in the study, the volumetric rate (Q). This characterizes the quantity of water parcels transported within the ocean due to the influence of AGW. Then the volumetric rate is calculated using the formula

$$
Q_n = 2\pi L h D_n \tag{5.4.76}
$$

This equation stands as a tool for quantifying the volumetric rate of water transport resulting from the intricate interplay of AGWs generated by submarine earthquakes. This equation encapsulates the dynamics that occur beneath the ocean's surface, where AGWs, embodying both acoustic and gravity wave characteristics, interact with the fluid medium. Delving into the representation of this equation provides insight into the intricate behaviour of AGWs and their ability to induce perturbations in the water column.

By computing the volumetric rate of water transport, this equation allows us to quantify the water movement by AGWs generated by submarine earthquakes. Such understanding is not only for unravelling the mechanics of these complex wave systems and the amount of water transported but also for assessing their potential impact on oceanic and atmospheric processes. As the depths of these phenomena continue to be explored, a testament to the depth of knowledge that can be extracted from the seemingly simple interactions shaping the planet's dynamics is provided by this equation.

Chapter 6

Results

6.1 Introduction

The primary objective of this work is to solve the complex interactions among submarine earthquakes and AGW and their impact on deep-water transport. Guided by this primary aim, I developed a mathematical model, which serves as a tool to calculate the results of this phenomenon. This model has been the basis of this work towards understanding AGW-induced water movements on a quantifiable scale. It is worth to note that at the fault location, the primary motion involves a direct displacement, resulting in a significant elevation of the water column that surpasses any influence attributable to acoustic propagation. For instance, similar to how the gravitational wave renders the acoustic contribution negligible at the surface, the fault region experiences a comparable phenomenon where the entire water column is uplifted at a consistent velocity. Consequently, the drift of acoustic waves within this region is disregarded due to its minor impact. Consequently, calculations within this area lack reliability, hence necessitating exclusion from focus.

This chapter embarks on the essential task of presenting and analyzing the outcomes of this research, focusing on quantifying the volume of water transported by AGWs. Beyond quantification, it delves into the invaluable role played by these waves in shaping oceanic water dynamics. Additionally, this chapter scrutinizes the contribution of each mode of these waves in different ocean depths, unveiling their varying significance in

influencing water transport processes

This chapter presents the core of the model-derived results where each figure and numerical insight showcased here serves as a testament to the commitment to knowing how much water can AGWs transport in the ocean within different depths. However, the calculation of how much water is being transported is also to see how important this transportation is to the oceans' health. Discussions about these discoveries will be carried out in the next chapter.

6.2 Case study: Sumatra earthquake submarine fault

As the research involves an investigation based on submarine earthquakes, The Sumatra 2004 event is considered as a prominent case study, representing a seismic occurrence that had a significant impact on the Earth's dynamics. This event was characterized by five major faults, each fault was split into two strips: one moving upwards while the other moved in the opposite direction [19]. Due to the unique nature and considerable magnitude of the fault system in this major seismic event and the availability of the data, this research was presented with an intriguing opportunity to delve into the influence of the AGWs within this intricate geophysical scenario.

The primary goal is to perform a detailed analysis of the volume of water transported by the AGWs generated by this submarine earthquake. By focusing on this specific submarine fault in the aftermath of the earthquake, this study seeks to gain an understanding of the AGW-induced water movements. This undertaking will show the role played by AGW in facilitating deepwater transport processes within the marine environment and to evaluate the importance of this transport in the context of ocean dynamics. Through this analysis, insights into the volume of water transported by AGWs originating from this fault are intended to be gained. This will allow an assessment of the magnitude of its influence compared to other sources. In the forthcoming sections, numerical insights and analyses that contributes to addressing this main research question will be presented. These findings collectively provide an understanding of the volume of water transported by AGW, specifically induced by the submarine fault connected to the Sumatra Earthquake. The investigative approach is structured in two stages: initially, by

parameter	Faults 1,2	Faults 3,4	Faults 5,6	Faults 7,8	Faults 9,10
Longitude	94.57°	93.90°	93.21°	92.60°	92.87°
Latitude	3.83°	5.22°	7.41°	9.70°	11.70°
L	110 km	75 km	195 km	75 km	175 km
b	65 km	65 km	60 km	47.5 km	47.5 km
Vertical upward	7.02 m	8.59 m	4.72 m	4.49 m	4.60 m
Vertical downward	-3.27 m	-3.84 m	-2.33 m	-2.08 m	-2.31 m
α	37°	12°	22°	4°	-10°
Duration	60 s	60 s	60 s	60 s	60 s

Table 6.1: Parameters of Sumatra 2004 event used in the study [19].

averaging over the entire depth, and subsequently, it is segmented into distinct layers of 400 m each. This approach offers a detailed analysis of the complex phenomena within the various layers.

6.3 Whole depth analysis

In light of the expansive area under study, which extends to a depth of 4,000 m, the investigative approach involves analyzing transport phenomena at varying depths and within distinct layers within this depth by averaging over the entire depth which will be carried out in this section. The study focuses on the contributions of the first 10 modes for all of the faults at different times, highlighting the intricate dynamics of these modes in water transport processes. To commence this analysis, an initial phase of assessment is initiated, spanning the entire depth profile.

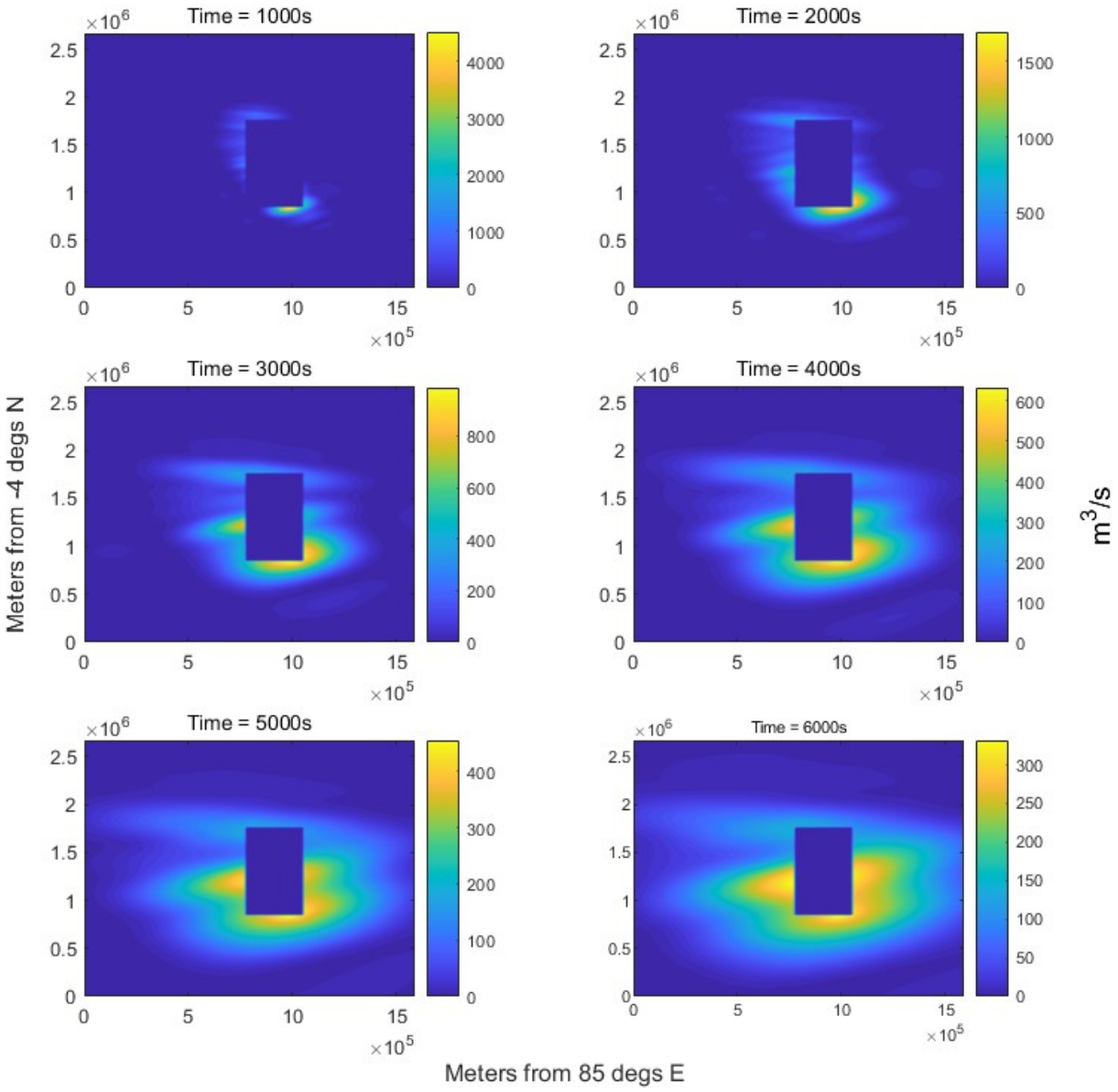

Figure 6.1: Volumetric water transport at different times averaged over the whole depth for Sumatra 2004 event.

Figure 6.1 shows a subplot comprising six individual plots, each revealing distinct facets of the volumetric rate of water transport. The data encompasses time intervals:

1000, 2000, 3000, 4000, 5000, and 6000 seconds following the initial eruption. To ensure accuracy and avoid computational inaccuracies, the calculations are performed outside the fault area. This approach allows for a more precise evaluation of AGW propagation characteristics once they exit the fault region. Consequently, the results and discussions on time intervals beyond the critical time are considered. The primary objective of figure 6.1 is to provide a visual representation of the temporal dynamics of water transport highlighting the influence of the first 10 AGW modes. In the near time of the eruption (1000 seconds),a substantial surge in water transport is observed, reaching a peak of approximately 4,606 m³/s.

Time (s)	Max. flow rate (m^3/s)
1000	4606.27
2000	1731.22
3000	1006.49
4000	644.75
5000	464.35
6000	338.68

Table 6.2: Maximum flow rates at different times

This surge underscores the instant and robust impact of processes generated by the earthquake, exemplifying the key role played by the AGWs. As time progresses, the data in table 6.2 illustrates a gradual decrease in the volume of the water transported. The data in figure 6.1 reveal a diminishing trend, signifying the waning intensity of water transport as time increases. However, it is crucial to note that water transport persists over extended durations. The figures convey that water is carried further away from the fault region, albeit with a reduced volume. This phenomenon vividly underscores the ability of the AGWs to transport water to distant areas, even as the intensity gradually diminishes.

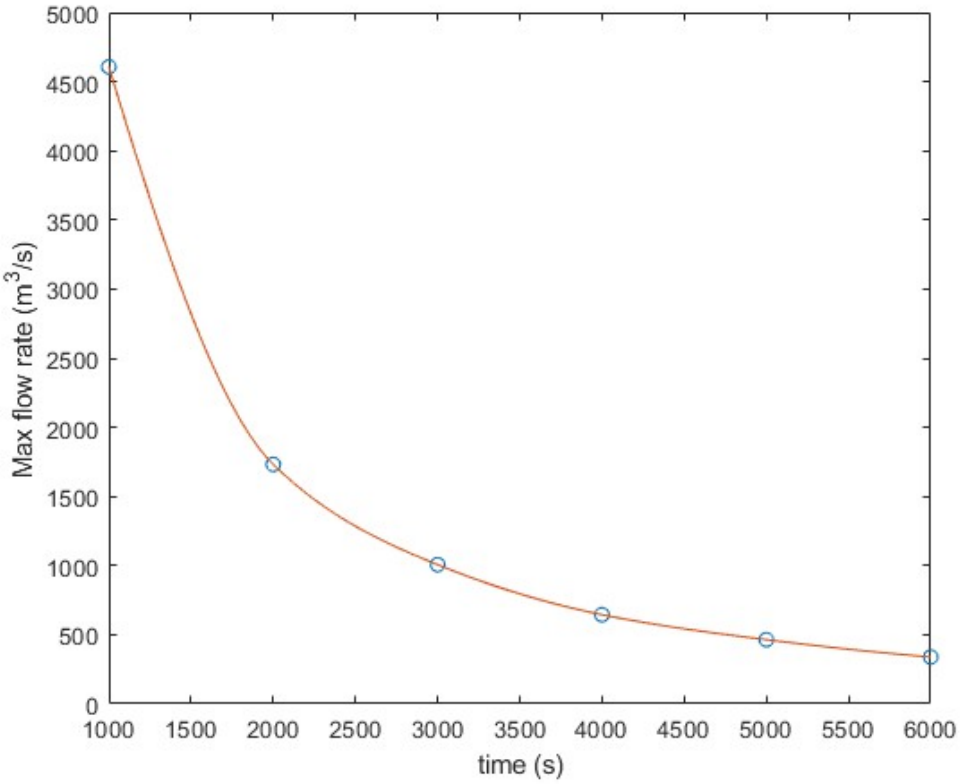

Figure 6.2: Maximum flow rate at various time intervals.

Figure 6.2 sheds light on the maximum flow rates of water and how it evolved after the Sumatra 2004 event. This helps to understand when water transport was at its highest and as these peaks decreased as time passed. Right after the earthquake (at 1000 s) the maximum flow rate of water is at its highest of all times, reflecting the immediate impact of the AGWs right after they were generated and their effect at the beginning. As time goes on, the data shows that these maximum flow rates gradually decrease. This trend indicates that the intensity of water transport becomes less as time passes. However, it's essential to note that water transport continues, even though it's not as intense for larger areas. Water keeps moving away from the fault zone, although with less force.

Figure 6.2 shows that the Sumatra 2004 event generated AGWs that created currents in the ocean, which decreased gradually over time. It gives an essential glimpse into how AGWs forces participate in shaping the region's dynamics after the earthquake.

looking at the mean drift velocities for these time intervals within the extensive study area it can be seen in figure 6.3 that the peak flow rate at 1000 s is at the forefront, symbolizing the initial fervour in post-seismic water movement by these waves.

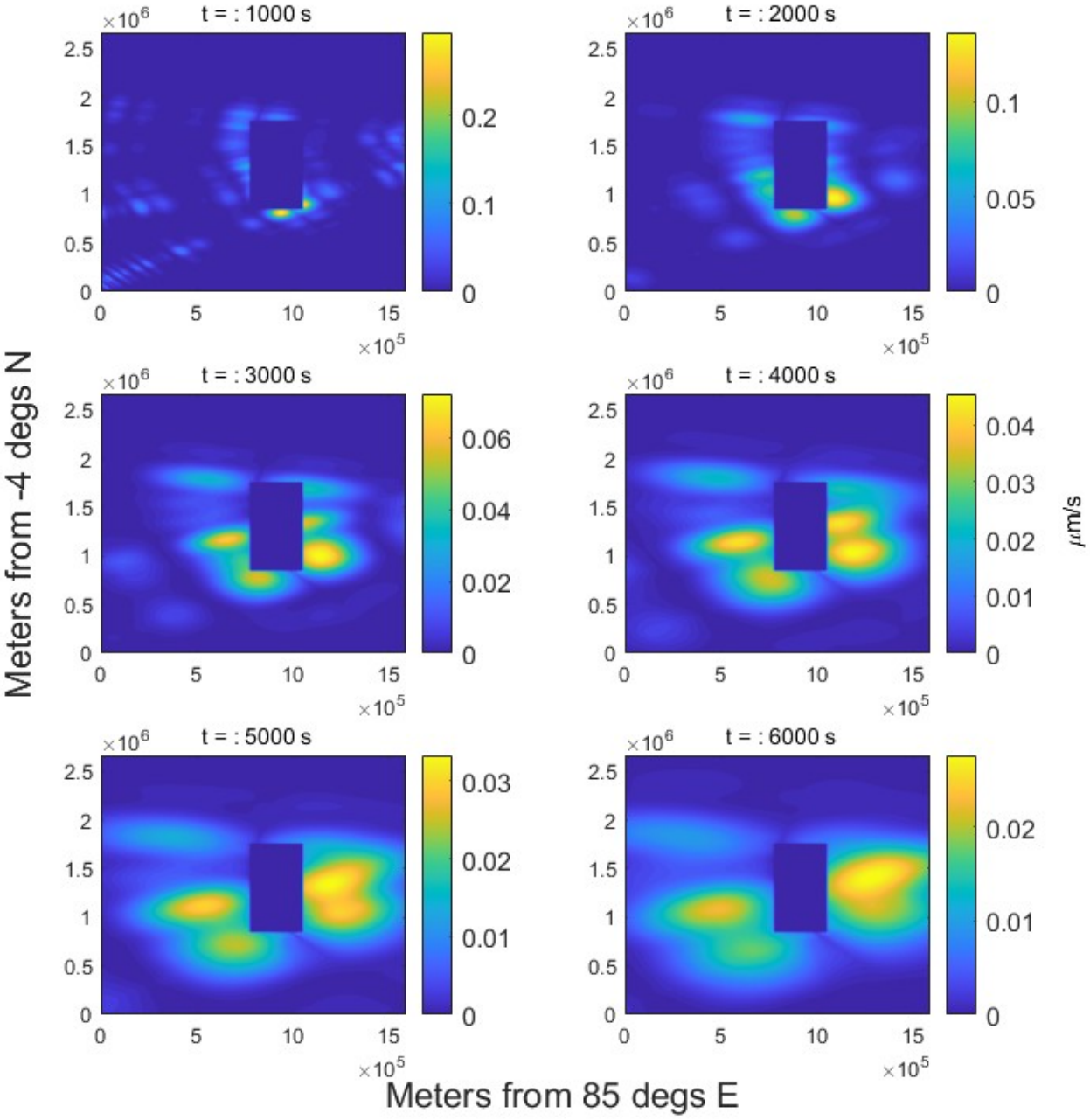

Figure 6.3: Contours of the magnitude of the drift velocities at different times averaged over the whole depth for Sumatra 2004 event.

Nonetheless, The seemingly small numerical values of these results are inherently influenced by the expansive scale of the research area despite their modest values. They cast insights into the multifaceted elements and their influence on fluid flow dynamics. Furthermore, the average MDV over time is scrutinized, offering insights into evolving water dynamics. These seemingly slow velocities are attributed to the fundamental physical processes governing the study, including the characteristics of AGWs and their role.

Using this to look at the average MDV over which offers a view of the overall drift patterns over the entire study period and reflects the changes in water movement over the specified period.

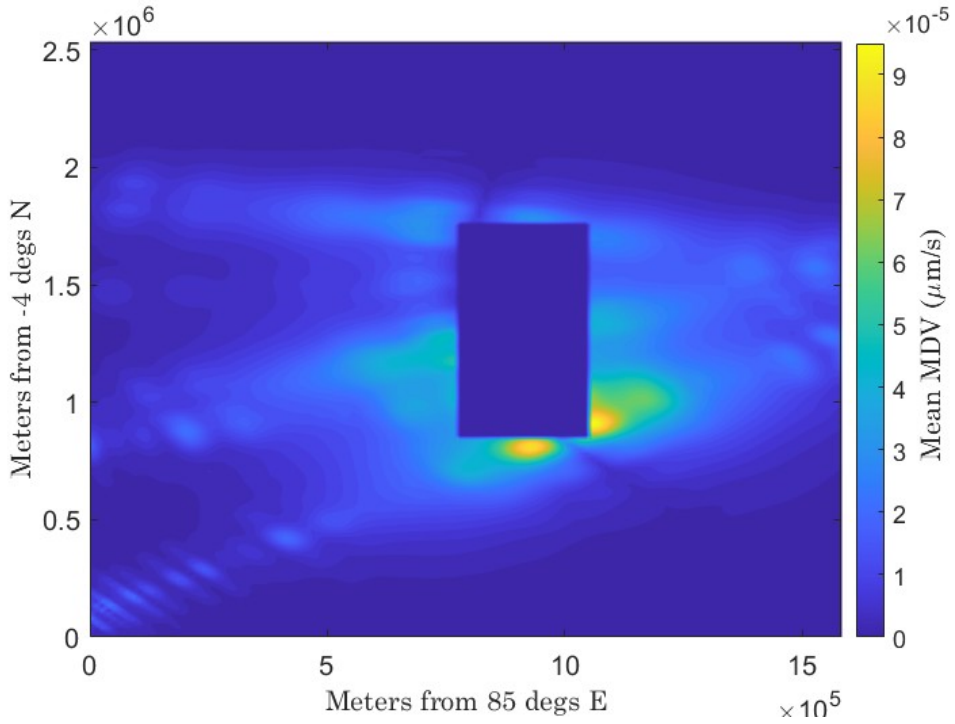

Figure 6.4: Contours of the magnitude of the average rate of mean drift velocity changes over time.

Figure 6.4 highlights the persistence and stability of water transport processes within the study area, especially when considering its vast geographical scale. While seemingly small, these values provide essential insights into the long-term dynamics of water

transport, which are of particular relevance in extensive geological and environmental contexts.

To gain an idea of the role played by individual modes in creating these water transports, an investigation into how each mode contributes is conducted. The aim is to gain a better understanding of which modes exert influence and which ones have a minimal impact on the overall dynamics of water transport by these waves. By scrutinising the interplay between modes and maximum flow rates, an intention is present to understand the underlying factors that govern the post-earthquake transport of water.

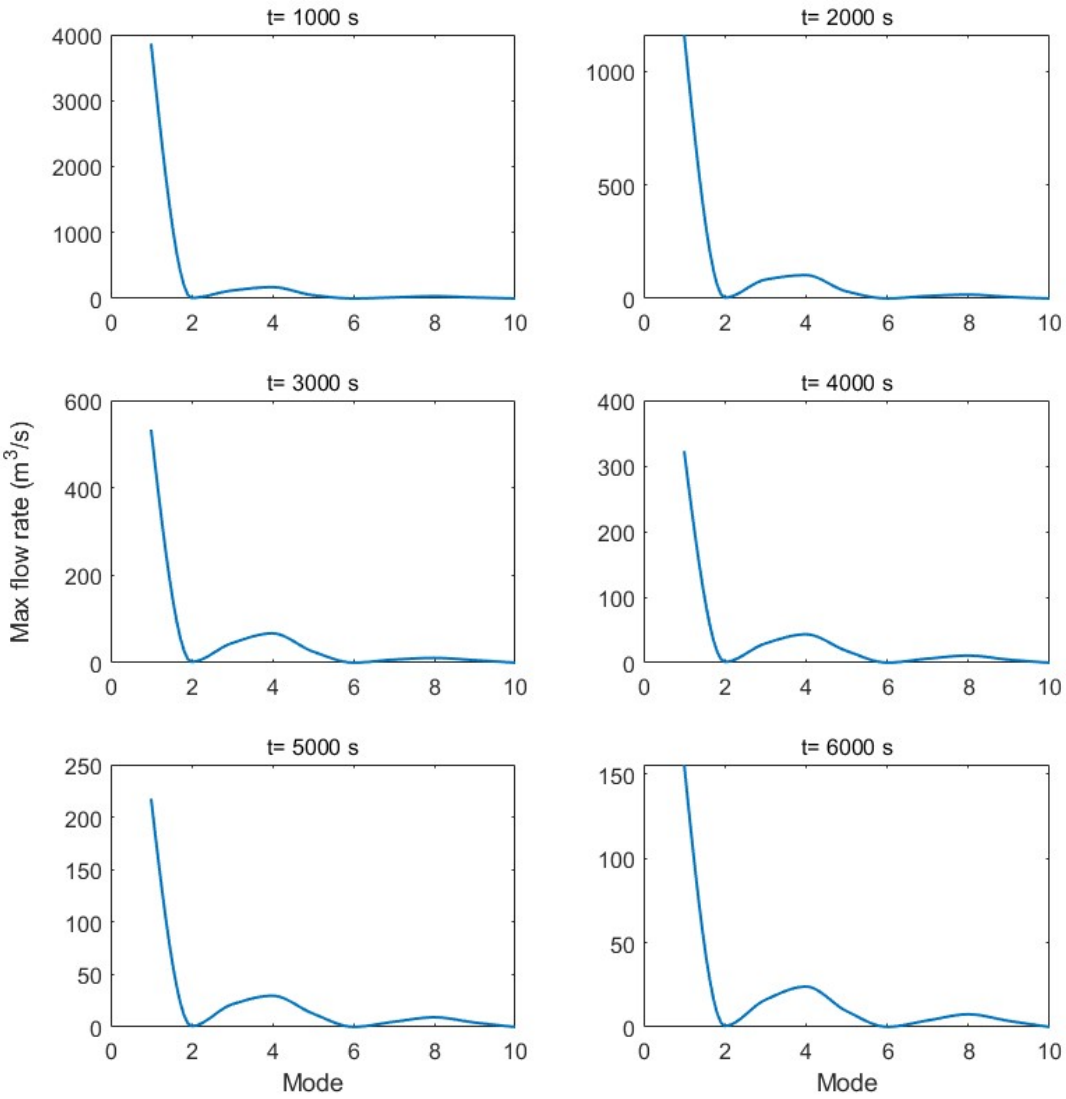

Figure 6.5: Maximum flow rate for AGW modes at different times.

Figure 6.5 illustrates the maximum flow rate and different modes after the Sumatra 2004 event. This sheds light on the distinctive contributions of each mode to water transport processes where it can be seen that the first mode significantly dominates the contributions, indicating its substantial role in water transport. As the modes are progressed through, varying contributions are observed, with the fourth mode, for instance,

exhibiting a higher contribution than the third, fifth, and second modes, indicating a non-linear pattern in their influence, although they remain noteworthy.

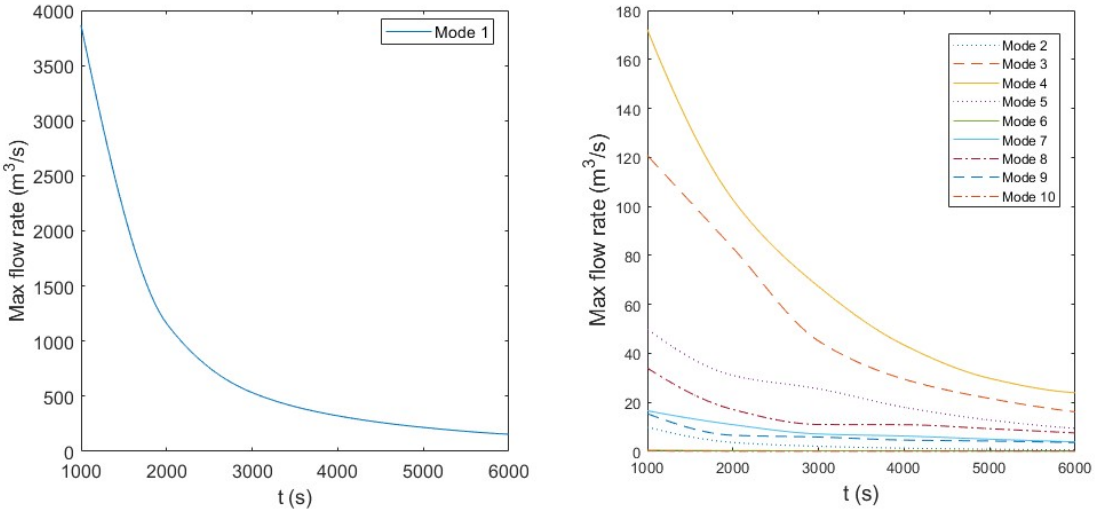

Figure 6.6: Temporal evolution of each mode's contribution to water transport over time.

However, it is seen in Table 6.3 that moving beyond the fifth mode, the contributions steadily diminish, becoming smaller. This observation underscores that the influence of the first mode stands out prominently, while the higher modes, especially beyond the fifth, have less impact on the overall water transport.

Mode \Time (s)	1000	2000	3000	4000	5000	6000
1	3865.52	1159.76	532.91	322.67	217.57	155.40
2	9.86	3.64	2.08	1.30	0.875	0.623
3	120.72	82.98	45.04	29.46	21.59	16.12
4	172.12	102.7	67.27	43.38	29.81	23.94
5	49.91	30.98	25.54	18	12.78	9.39
6	0.474	0.291	0.235	0.184	0.138	0.104
7	16.57	10.9	7.10	6.28	5	3.9
8	34	17.08	10.98	10.88	9.26	7.52
9	15.36	6.58	5.85	4.61	4.22	3.58
10	0.179	0.084	0.071	0.047	0.046	0.041

Table 6.3: Max flow rate (m^3/s) of each mode at each time.

This provides an insight into the hierarchical distribution of contributions among the modes, which helps to discern the primary drivers of water transport following the event.

Figure 6.6 shows the dynamic temporal evolution of each mode's contribution to water transport. The first plot shows the contribution of the dominant first mode, illuminating its role in water movement. The second plot offers a view of how the remaining modes exhibit varying contributions underscoring the intricate interplay among these modes. This underscores the non-linear patterns in the contributions of the various modes, unveiling the changing relevance of these modes. This shows how different modes impact the dynamics of water transport over time.

In conclusion, the analysis focused on quantifying the volumetric rates of water transport by AGWs across the entire depth profile. The findings highlight the impact of AGWs in inducing rapid and immediate water transport following the earthquake. Volumetric rates gradually decreased over time, illustrating the evolving nature of water transport in the post-seismic phase. Examination of mode contributions revealed the

consistent dominance of the first mode among other modes. These insights are important for understanding the complexities of water transport dynamics and the role of AGWs. Now, attention will be turned to the analysis of various depth layers., uncovering the nuanced dynamics that occur within distinct strata. These insights contribute to the understanding of water transport complexities and its interaction with AGWs generated by geological forces.

6.4 Different depths analysis

In continuation of analyzing the role of AGWs throughout the entire depth, the study now proceeds to a more detailed analysis. At this stage, the depth range will be subdivided into ten layers of 400 m each, creating a more refined portrait of AGWs' influence in the ocean's varying strata. This approach provides us with a closer examination of how AGWs exert their influence at different depth layers, allowing us to discern their distinctive contributions and understand their influence on water transport within these layers. This analysis focuses on the time at t= 1000 s to enable us to capture the AGWs' impact during the critical early phase when volumetric flow rates are at their peak.

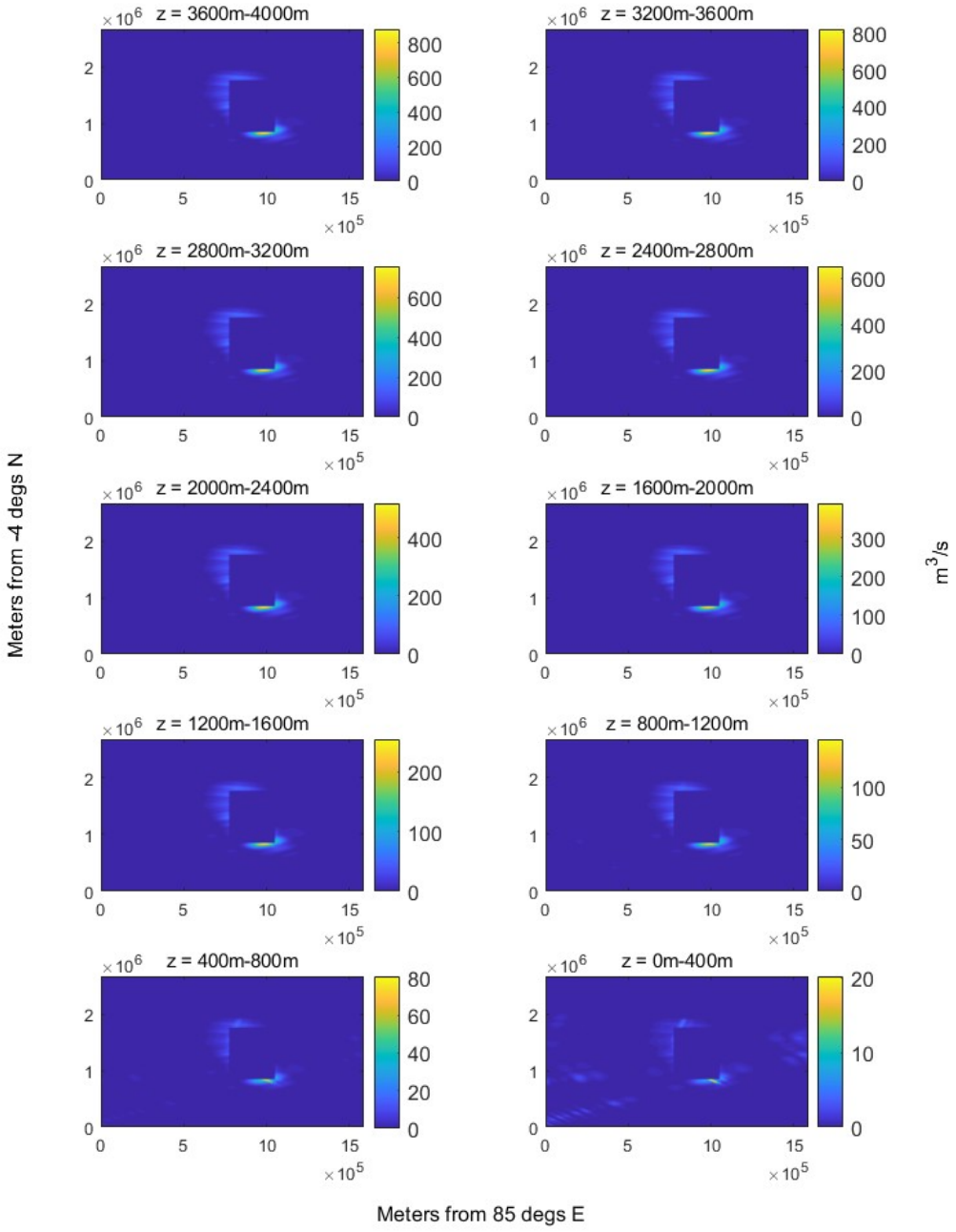

Figure 6.7: Contours of the magnitude of the volumetric rate of water transport at t= 1000 s averaged over layers of 400 m for Sumatra 2004 event.

Figure 6.7 shows the volumetric rate of water transport within layers of $400m$ which notably illustrates the considerable influence of AGWs across all layers. These waves are instrumental in facilitating the movement of water, particularly in the surface and near-surface layers.

z (m)	Max flow (m^3/s)
3600-4000	896
3200-3600	837.18
2800-3200	772.88
2400-2800	663.86
2000-2400	528.84
1600-2000	395.78
1200-1600	259.83
800-1200	148.98
400-800	82.27
0-400	20.61

Table 6.4: Max flow rate in different layers at t= 1000 s.

A notable observation involves the differences in flow rates between the surface layer and the deeper layers, as highlighted in Table 6.4. This disparity becomes particularly evident when considering the discernible decline in flow rate over time. Despite this variation, it can be seen that the distance that water is transported remains relatively uniform across some of the layers as we see in Figure 6.7.

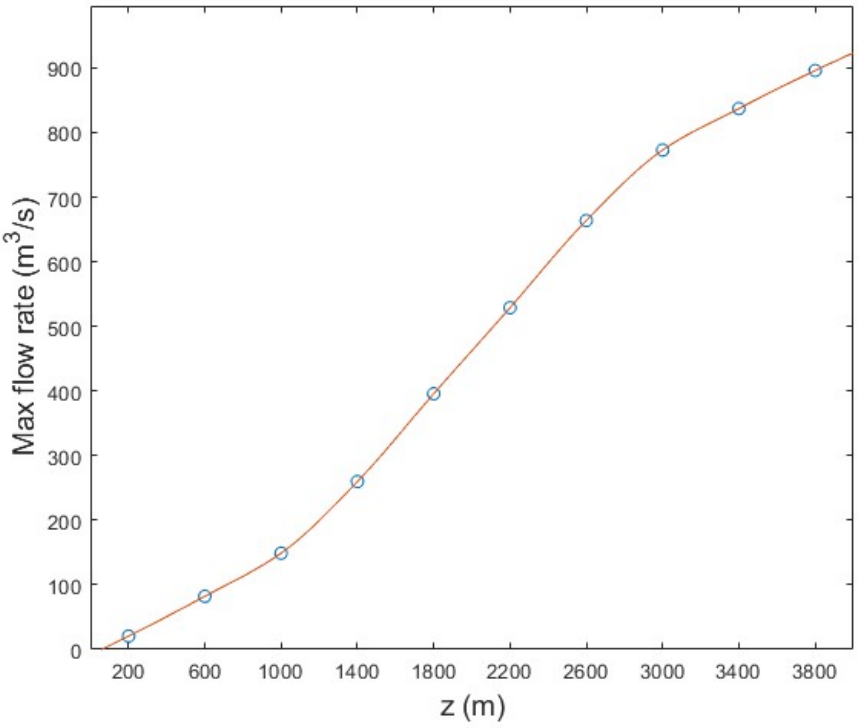

Figure 6.8: Volumetric rate of water transport at t= 1000 s for layers of 400 m for Sumatra 2004 event.

This observation underscores the remarkable capability of AGWs to transport water both in the deep ocean and in proximity to the ocean's surface. Moreover, it aligns with the findings of [22], which indicated that AGWs play a crucial role in enhancing water flow in all depths as corroborated by figure 6.8.

This analysis shows the contribution of AGWs in water transport across ocean layers, highlighting their role in influencing the transport in all depths and not only near the surface. To offer more insights into how water is distributed at different ocean depths the mean drift velocity is presented next for the layers under consideration.

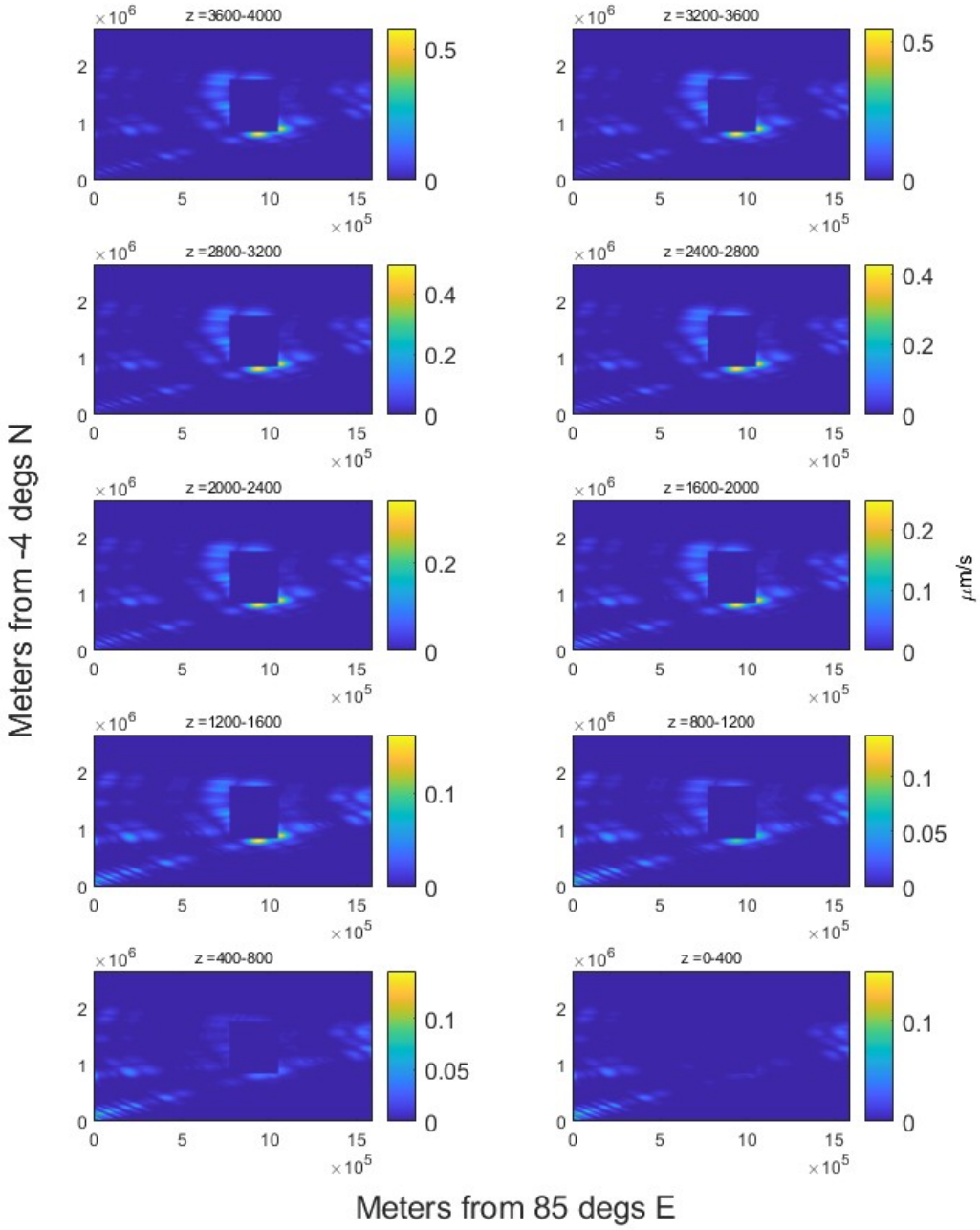

Figure 6.9: Contours of the magnitude of the mean drift velocities at t= 1000 s for different layers of 400 m for Sumatra 2004 event.

At the time t= 1000 s, it can be seen that the mean drift velocity, with some differences between depths, exhibits distinct patterns, showing higher velocity near the surface that decreases with depth. The results show the role of AGWs in influencing water transport in all depths. While the mean drift velocity helps to understand the general pattern, it's the AGWs that provide the driving force behind these velocity variations. Their interactions within the ocean contribute to the observed dynamics, where water parcels are shifted more vigorously near the surface but also experience movement at greater depths. Overall, these findings shed light on the dynamic interplay between water layers within the ocean, driven by AGWs, and how they impact the water distribution across different depths, thus enhancing the comprehension of the complex water transport processes within different ocean layers. Across all depths, a clear pattern emerges: the first mode stands out as the dominant contributor, exerting substantial influence on water transport as it is shown in figure 6.10. This observation aligns with the notion that the first mode often plays a pivotal role in transporting water in oceans. When delving into the depths closer to the ocean floor, it appears that all modes exhibit more or less similar contributions. This finding underscores the remarkable strength of the first mode, which, even in proximity to the ocean bottom, retains its dominant position in influencing water transport processes. Moreover, this outcome reaffirms the earlier observations from the previous sections, where the fourth and third modes demonstrate slightly more impact than the second mode, although the differences are relatively subtle. Moving beyond the fifth mode, it is noted that contributions become smaller and might be negligible. This aligns with existing knowledge that the higher-order modes often play a minor role in these processes. Overall, this analysis deepens the understanding of how different modes influence water transport at varying depths, with the first mode consistently emerging as the most influential, a pattern consistent with the previous findings.

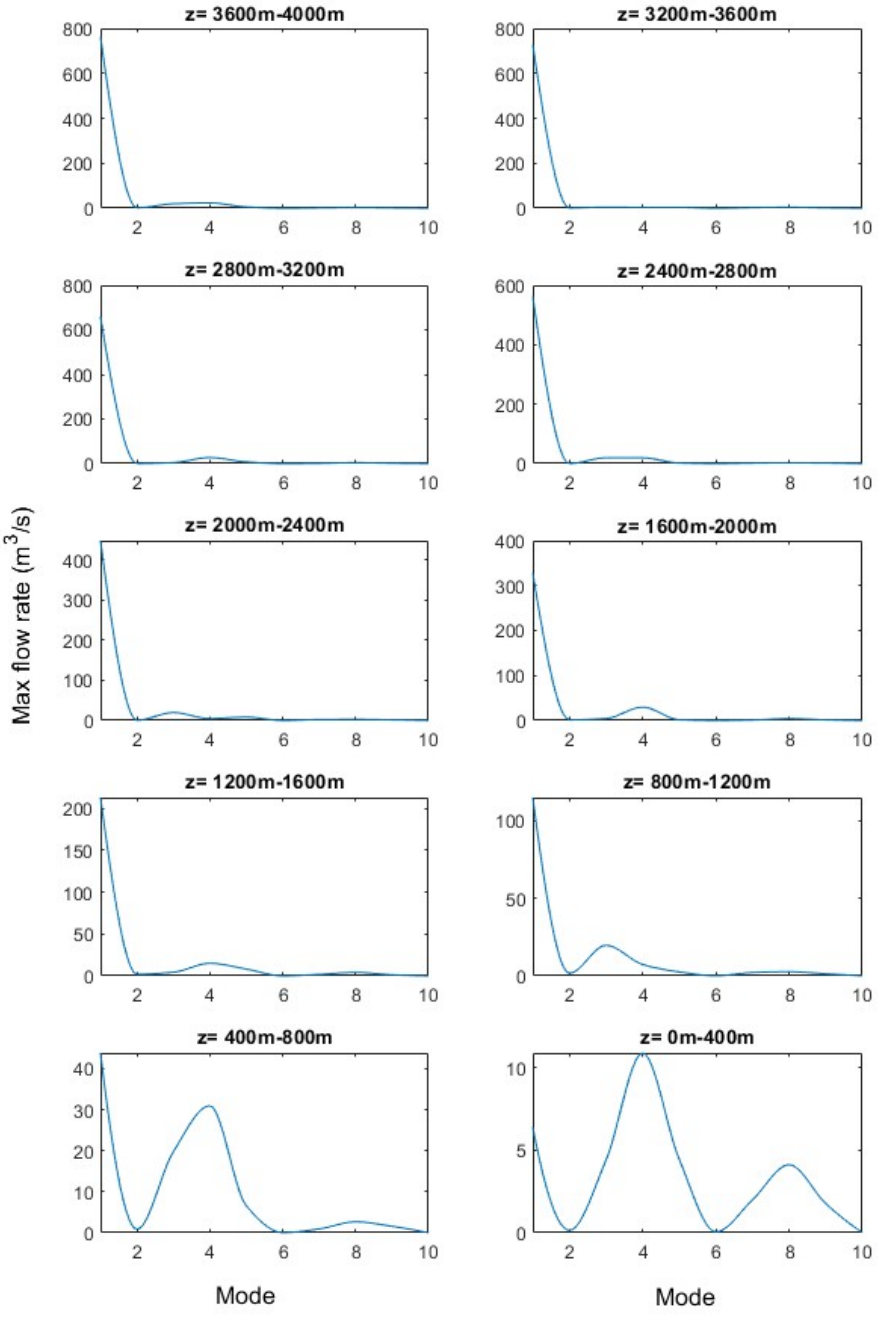

Figure 6.10: Maximum contribution of each mode in different depth layers.

Chapter 7

Discussion and Summary

In this chapter, a discussion of the key findings from this research is engaged, delving into their implications and significance. Subsequently,concise summary of the primary contributions made by this study is provided.

7.1 Key Findings and Implications

7.1.1 Volumetric Flow Rate and Water Transport

This research delves into volumetric flow rates in the early stages, revealing intriguing patterns that provide invaluable insights into water transport dynamics. These findings emphasize the pivotal role of AGWs in governing the tempo of water dynamics, especially in early times after the earthquake. Of particular significance is the flow rate observed during the early post-seismic phase signifying the remarkable amount of water in this initial period, a testament to its swift response to seismic disturbances.

To put this into perspective, the Mississippi River is the 15^{th} largest river globally, as it is discharging around 16,792 m^3/s [6]. The volumetric flow rate at the early phase is approximately 4,606 m^3/s which is comparable to the flow of the Mississippi at certain points along its course and this is equivalent to 21.44% of the flow of the river. In essence, the flow due to AGWs generated by the Sumatra 2004 event rivals that of a ma-

jor river, highlighting its role in oceanic water transport. This comparison underscores the substantial impact of AGWs in transporting water, and it is crucial for the life of the oceans.

7.1.2 AGWs and Their Influence

The study of the contribution of AGWs to water transport across different depth layers shows the role of AGWs in the oceans. Surface waves dominate water transport near the surface, and the findings reveal that AGWs play a substantial role in water transport near the surface and in the deeper layers, as evidenced by the disparities in flow rates between these regions.

This observation highlights the remarkable capacity of AGWs to transport water both in the deep ocean and near the ocean's surface, corroborating the findings of [22] which emphasized the crucial role of AGWs in enhancing water flow, especially in proximity to the ocean's surface. It sheds light on the intricate interplay between AGWs and water transport across different layers of the ocean, emphasising their pivotal role in governing fluid movement within this complex aquatic environment.

7.2 Main Contributions of the Research

In summary, this research has made contributions to the field of ocean dynamics and water transport:

1. Insights into Flow Rate: these findings have provided insight into the role of the AGWs generated by submarine earthquakes in governing the dynamics of water transport as they contribute in transporting water in all depths and not only near the surface. This helps to understand how water moves within the ocean, shedding light on the swift response of water to seismic disturbances and its implications for various oceanic processes.

2. Understanding AGWs: This study has deepened the understanding of AGWs generated by submarine earthquakes and their role in water transport as it showed how they contribute in transporting water in deep ocean. It demonstrates that these types of

waves are not limited to surface water transport, but also contribute to flow dynamics in deeper layers of the ocean in an amount comparable to other mechanisms.

3. Complex Interplay of Forces: Examining the contributions of different modes within distinct depth layers shows the differences in contribution between modes and how some are participating more than others. The dominance of the first mode and the variations in mode contributions have provided an understanding of the underlying dynamics.

7.3 Significance of the Research

The primary aim of this research is to quantitatively assess the water transport induced by AGWs generated by submarine earthquakes, and the findings provide a foundation for future investigations into the complex interplay between AGWs generated by geological forces and fluid dynamics in oceanic environments which advances the understanding of water transport processes in the context of seismic events that generate AGWs. In principle, the frequent occurrence of submarine earthquakes, leading to the generation of AGWs, can produce significant water currents with volumetric flow rates as substantial as tens of Sverdrups. These rates are comparable to the transport capacity of other major ocean current systems. these are crucial for plankton, algae, bacteria, microorganisms, and various marine organisms populating the deep oceans, as they advantage of the small drifting microorganisms, that are unable to swim against a current [25], to gain access to larger areas, increasing their opportunities for locating food. Moreover, the larger marine animals benefit from the constant transportation of salt, carbon, nutrients, and other substances carried by the current. This continuous flow is especially vital for sessile creatures, such as carnivorous sponges, inhabiting the deep ocean at depths exceeding 8000 m [47].

7.4 Further work

This study has presented a model that gives quantitative insights into water transport by acoustic gravity waves generated by submarine earthquakes, However, there remain

avenues for further exploration in this field. It is imperative to underscore the necessity of validating the obtained solutions with existing numerical models. For instance, Abdolali et al. (2015) [1] present a comprehensive numerical model that elucidates various aspects of the phenomenon under investigation. By comparing the results with such established models, we can ascertain the robustness and accuracy of the findings. future research endeavours should prioritise such validation exercises to enhance the reliability and applicability of the proposed solutions.

Also, incorporating additional factors could offer more understanding of this transportation within the ocean. For example, viscosity, as it plays a role in determining the resistance of water to flow and may influence the observed drift velocities.

Moreover, the elasticity of the ocean floor is another aspect that warrants attention in future investigations to examine the impact of elasticity on the propagation of acoustic gravity waves. Accounting for the elasticity of the seafloor could introduce a new dimension to the understanding of AGW-induced water movements, particularly in relation to the interaction between these waves and the ocean floor.

Extending the research to include such factors can enhance the accuracy and applicability of the model, providing a more perspective on the intricate processes governing water transport by AGWs.

In contemplating the broader implications of these findings, there lies a speculative avenue concerning the influence of AGWs on deep ocean currents by other mechanisms. Particularly within regions proximate to submarine faults susceptible to seismic activity, AGWs may play a contributory role within the circulation patterns of the deep ocean. This conjecture can open the door for subsequent research, aimed at elucidating the manner in which these AGWs might exert influence on the ocean circulations within these earthquake zones.

These considerations open avenues for continued exploration and refinement of the understanding of AGWs generated by submarine earthquakes and their role in deep ocean currents.

Bibliography

[1] Abdolali, A., Kirby, J. and Bellotti, G. [2015], 'Depth-integrated equation for hydro-acoustic waves with bottom damping', *Journal of Fluid Mechanics* **766**.

[2] Abdolali, A. and Kirby, J. T. [2017], 'Role of compressibility on tsunami propagation', *Journal of Geophysical Research: Oceans* **122**.

[3] Abel, D. and McConnell, R. [2009], *Environmental Oceanography: Topics and Analysis*, Jones & Bartlett Learning.

[4] Abramowitz, M. and Stegun, I. A. [1965], *Handbook of mathematical functions: with formulas, graphs, and mathematical tables*, Vol. 55, Courier Corporation.

[5] Bender, C. and Orszag, S. [1999], *Advanced Mathematical Methods for Scientists and Engineers I: Asymptotic Methods and Perturbation Theory*, Advanced Mathematical Methods for Scientists and Engineers, Springer.

[6] Bolonkin, A. [2013], 'Electron hydro electric generator', *Int J Adv Eng Appl ISSN* pp. 2321–7723.

[7] Bolt, B. [2004], *Earthquakes and Geological Discovery*, DIANE Publishing Company.

[8] Boyd, P. W. and Doney, S. C. [n.d.], 'Modelling regional responses by marine pelagic ecosystems to global climate change', *Geophysical Research Letters* **29**(16), 53–1–53–4.

[9] Chelton, D. B., Schlax, M. G. and Samelson, R. M. [2011], 'Global observations of nonlinear mesoscale eddies', *Progress in Oceanography* **91**(2), 167–216.

[10] Chris, S., Feely, R., Gruber, N., Key, R., Lee, K., Bullister, J., Wanninkhof, R., Wong, C., Wallace, D., Tilbrook, B., Millero, F., Peng, T.-H., Kozyr, A., Ono, T. and Rios, A. [2004], 'The oceanic sink for anthropogenic co2', *Science (New York, N.Y.)* **305**, 367–71.

[11] Colling, A. [2001], *Ocean circulation*, Vol. 3, Butterworth-Heinemann.

[12] Condie, K. C. [1997], Preface, *in* K. C. Condie, ed., 'Plate Tectonics and Crustal Evolution (Fourth Edition)', fourth edition edn, Butterworth-Heinemann, Oxford, pp. ix–x.

[13] Dalrymple, R. and Rogers, B. [2007], A note on wave celerities on a compressible fluid, pp. 3–13.

[14] Dean, R. and Dalrymple, R. [1991], *Water Wave Mechanics for Engineers & Scientists*, World Scientific.

[15] Dhanak, M. and Xiros, N. [2016], *Springer Handbook of Ocean Engineering*, Springer Handbooks, Springer International Publishing.

[16] Ferrari, R. and Wunsch, C. [2009], 'Ocean circulation kinetic energy: Reservoirs, sources, and sinks', *Annual Review of Fluid Mechanics* **41**.

[17] Gerya, T. [2019], *Introduction to numerical geodynamic modelling*, Cambridge University Press.

[18] Gradshteyn, I. S. and Ryzhik, I. M. [2014], *Table of integrals, series, and products*, Academic press.

[19] Grilli, S., Ioualalen, M., Asavanant, J., Shi, F. and Kirby, J. [2007], 'Source constraints and model simulation of the december 26, 2004, indian ocean tsunami', *Journal of Waterway Port Coastal and Ocean Engineering-asce - J WATERW PORT COAST OC-ASCE* **133**.

[20] Gruber, N., Gloor, M., Mikaloff Fletcher, S. E., Doney, S. C., Dutkiewicz, S., Follows, M. J., Gerber, M., Jacobson, A. R., Joos, F., Lindsay, K. et al. [2009], 'Oceanic sources, sinks, and transport of atmospheric co2', *Global Biogeochemical Cycles* **23**(1).

[21] Hendin, G. and Stiassnie, M. [2013], 'Tsunami and acoustic-gravity waves in water of constant depth', *Physics of Fluids* .

[22] Kadri, U. [2014], 'Deep ocean water transport by acoustic-gravity waves', *Journal of Geophysical Research: Oceans* .

[23] Kadri, U. and Stiassnie, M. [2013*a*], 'Generation of an acoustic-gravity wave by two gravity waves, and their subsequent mutual interaction', *Journal of Fluid Mechanics* **735**.

[24] Kadri, U. and Stiassnie, M. [2013*b*], 'A note on the shoaling of acousticgravity waves', *WSEAS Transactions on Fluid Mechanics* **8**(2), 43–49.

[25] Lalli, C. and Parsons, T. R. [1997], *Biological Oceanography: An Introduction*, Butterworth-Heinemann, Oxford, U. K.

[26] Landau, L. D. and Lifshitz, E. M. [1987], *Fluid Mechanics, Second Edition: Volume 6 (Course of Theoretical Physics)*, Butterworth-Heinemann.

[27] Lighthill, M. and Lighthill, J. [2001], *Waves in Fluids*, Cambridge Mathematical Library, Cambridge University Press.

[28] Longuet-Higgins, M. S. [1950], 'A Theory of the Origin of Microseisms', *Philosophical Transactions of the Royal Society of London. Series A, Mathematical and Physical Sciences* **243**(857), 1–35. Publisher: The Royal Society.

[29] Mathewson, C. [1981], *Engineering Geology*, Merrill.

[30] Mathez, E. A. and Webster, J. D. [2004], *The earth machine: the science of a dynamic planet*, Columbia University Press.

[31] Mei, C. C. and Kadri, U. [2018], 'Sound signals of tsunamis from a slender fault', *Journal of Fluid Mechanics* **836**, 352–373.

[32] Neumann, G. [2014], *Ocean currents*, Vol. 4, Elsevier.

[33] Phillips, O. M. [1977], *The dynamics of the upper ocean*, Cambridge university press.

[34] Pichon, X., Francheteau, J. and Bonnin, J. [2013], *Plate Tectonics*, Developments in Geotectonics, Elsevier Science.

[35] Publishing, B. and Rafferty, J. [2010], *Plate Tectonics, Volcanoes, and Earthquakes*, Dynamic Earth, Britannica Educational Publishing.

[36] Qiu, C., Mandt, S. and Rudolph, M. [2020], 'Variational dynamic mixtures', *CoRR* **abs/2010.10403**.

[37] Rahmstorf, S. [2003], 'Thermohaline circulation: The current climate', *Nature* **421**(6924), 699–699.

[38] Roemmich, D., Alford, M. H., Claustre, H., Johnson, K., King, B., Moum, J., Oke, P., Owens, W. B., Pouliquen, S., Purkey, S. et al. [2019], 'On the future of argo: A global, full-depth, multi-disciplinary array', *Frontiers in Marine Science* **6**, 439.

[39] Siegenthaler, U. and Sarmiento, J. [1993], 'Atmospheric carbon dioxide and the ocean', *Nature* **365**(6442), 119–125.

[40] Silverstein, A., Silverstein, V. B. and Nunn, L. S. [2009], *Plate tectonics*, Twenty-First Century Books.

[41] Sloyan, B. and Rintoul, S. [2001], 'The southern ocean limb of the global deep overturning circulation', *Journal of Physical Oceanography - J PHYS OCEANOGR* **31**, 143–173.

[42] Smetacek, V. [1999], 'Diatoms and the ocean carbon cycle', *Protist* **150**(1), 25–32.

[43] Steele, J. H., Thorpe, S. A. and Turekian, K. K. [2010], *Ocean Currents: A derivative of the encyclopedia of Ocean Sciences*, Academic Press.

[44] Talley, L., Pickard, G., Emery, W. and Swift, J. [2011], 'Descriptive physical oceanography: An introduction: Sixth edition', *Descriptive Physical Oceanography: An Introduction: Sixth Edition* pp. 1–555.

[45] Thompson, D. W. and Solomon, S. [2002], 'Interpretation of recent southern hemisphere climate change', *Science* . Accessed November 13, 2023.

[46] Turekian, K. and Bacon, M. [2003], 6.12 - geochronometry of marine deposits, *in* H. D. Holland and K. K. Turekian, eds, 'Treatise on Geochemistry', Pergamon, Oxford, pp. 321–341.
URL: *https://www.sciencedirect.com/science/article/pii/B0080437516061132*

[47] Vacalet, J. and Boury-Esnault, N. [1995], 'Carnivorous sponges', *Nature* **373**, 26–43.

[48] Visser, A. W. [2007], 'Biomixing of the oceans?', *SCIENCE-NEW YORK THEN WASHINGTON-* **316**(5826), 838.

[49] Williams, B. and Kadri, U. [2018], 'Acoustic-gravity waves from slender faults'.

[50] Williams, B. and Kadri, U. [2023], 'On the propagation of acoustic–gravity waves due to a slender rupture in an elastic seabed', *Journal of Fluid Mechanics* **956**.

[51] Williams, B., Kadri, U. and Abdolali, A. [2021], 'Acoustic–gravity waves from multi-fault rupture', *Journal of Fluid Mechanics* **915**, A108–undefined.

[52] Wong, R. [2001], *Asymptotic Approximations of Integrals*, Classics in Applied Mathematics, Society for Industrial and Applied Mathematics.

[53] Wunsch, C. and Ferrari, R. [2004], 'Vertical mixing, energy, and the general circulation of the oceans', *Annu. Rev. Fluid Mech.* **36**, 281–314.

[54] Yamamoto, T. [1982], 'Gravity waves and acoustic waves generated by submarine earthquakes', *International Journal of Soil Dynamics and Earthquake Engineering* **1**(2), 75–82.